

Original Article

Cite this article: Sepahi AA, Vahidpour H, Lentz DR, McFarlane CM, Maanijou M, Salami S, Miri M, Mansouri M, and Mohammadi R (2020) Rare sapphire-bearing syenitoid pegmatites and associated granitoids of the Hamedan region, Sanandaj–Sirjan zone, Iran: analysis of petrology, lithogeochemistry and zircon geochronology / trace element geochemistry. *Geological Magazine* **157**: 1499–1525. <https://doi.org/10.1017/S0016756820000023>

Received: 3 June 2019

Revised: 15 December 2019

Accepted: 3 January 2020

First published online: 24 February 2020

Keywords:

sapphire; syenitoid; zircon geochemistry; geochronology; pegmatite; Sanandaj–Sirjan; Iran

Author for correspondence:

Ali A Sepahi,
Emails: aasepahi@gmail.com,
sepahi@basu.ac.ir

Rare sapphire-bearing syenitoid pegmatites and associated granitoids of the Hamedan region, Sanandaj–Sirjan zone, Iran: analysis of petrology, lithogeochemistry and zircon geochronology / trace element geochemistry

Ali A Sepahi¹ , Hamed Vahidpour¹, David R Lentz², Chris RM McFarlane², Mohammad Maanijou¹, Sedigheh Salami¹, Mirmohammad Miri³, Mehrak Mansouri¹ and Razieh Mohammadi¹

¹Department of Geology, Bu-Ali Sina University, Shahid Ahmadi Roshan St., Hamedan, 65174-33391, Iran;

²Department of Earth Sciences, University of New Brunswick, 2 Bailey Drive, Fredericton, New Brunswick E3B 5A3, Canada and ³Department of Geology, Faculty of Earth Sciences, Shahid Chamran University of Ahvaz, Ahvaz, Iran

Abstract

Pegmatites and associated granitoids are integral parts of the Alvand plutonic complex in the Sanandaj–Sirjan zone, Iran. Whole rock major- and trace-element lithogeochemistry together with zircon U–Pb geochronology and zircon geochemistry are examined to evaluate the petrogenesis of sapphire-bearing pegmatites and other peraluminous pegmatites in the region. Pegmatites vary in their chemical compositions from mostly peraluminous, high-K calc-alkaline to shoshonitic signatures. A rare variety of extremely peraluminous sapphire-bearing syenitoid pegmatite ($\text{Al}_2\text{O}_3 > 30$ wt %; $\text{A}/\text{CNK} > 2$) exists. This silica-undersaturated pegmatite and its sapphire crystals have a primary igneous origin. U–Pb zircon geochronology of three separate samples from this pegmatite indicates the following ages: 168 ± 1 Ma, 166 ± 1 Ma and 164 ± 1 Ma. The zircon grains have notable amounts of Hf (up to 17 200 ppm), U (up to 13 580 ppm), Th (up to 5148 ppm), Y (up to 4764 ppm) and ΣREE (up to 2534 ppm). There is a positive correlation between Hf and Th, Nb and Ta, U and Th, and Y and HREE and a negative correlation between Hf and Y values in the zircons. These zircons exhibit pronounced positive Ce anomalies ($\text{Ce}/\text{Ce}^* = 1.15\text{--}68.06$) and negative Eu anomalies ($\text{Eu}/\text{Eu}^* = 0.001\text{--}0.56$), indicative of the relatively oxidized conditions of the parent magma. Ti-in-zircon thermometry reveals temperatures from as low as ~ 683 °C up to ~ 828 °C (average = 755 ± 73 °C). Zircon and monazite saturation equilibria are also consistent with these temperatures. Zircon grains are magmatic (average $\text{La} < 1.5$, $(\text{Sm}/\text{La})_{\text{N}} > 100$ and $\text{Th}/\text{U} > 0.7$), with chemical characteristics similar to zircons from continental crust.

1. Introduction

Petrogenetic studies on various types of pegmatites and aplites are quite common in the recent literature and are reported from many countries worldwide (e.g. London, 2005, 2008, 2014a; Simmons & Webber, 2008; Nabelek *et al.* 2010; Cerný *et al.* 2012; London & Morgan, 2012; Thomas *et al.* 2012; Dill, 2015; Thomas & Davidson, 2015). Pegmatitic bodies in most places are small in volume, but are texturally and mineralogically diverse. In recent years, the subjects of occurrence, origin and generation, crystallization history, classification, geological evolution, and ore-forming processes, which result in the generation of rare metals as well as industrial minerals and gemstones, have been the main target of the science of pegmatology (e.g. London, 2008, 2018). Semi-precious gemstones, such as some varieties of garnet, tourmaline and beryl, are reported from many places northwest of the Sanandaj–Sirjan zone (SSZ) (Nouri *et al.* in press), but sapphire occurs only in the Hamedan region. So far, only in a Persian paper (Sheikhi-Gheshlaghi & Ahmadi, 2015) have sapphire-bearing pegmatites (SBPs) been reported to exist in the region, but with no discussion of their possible genetic link with other pegmatites and associated granitoids. The region can be potentially important for the exploration of sapphire-bearing pegmatite dykes as sources for gem quality deposits. In other areas in the NW SSZ (i.e. Boroujerd and Qorveh) the occurrence of SBPs has not been reported yet.

The SSZ is a major tectono-stratigraphic unit in Iran that occurs between the Zagros fold-thrust belt (to the SW) and Central Iran zone (to the NE). The SSZ is mainly composed of Upper Palaeozoic to Mesozoic meta-sedimentary sequences, which have been deformed during Mesozoic and Cenozoic tectonic events. For this zone, only a few published studies of

pegmatites/aplites exist (e.g. Sepahi *et al.* 2018). In some places the SSZ pegmatites intrude plutonic and metamorphic complexes, but in most places they are simple granitic pegmatites, and those with syenitic composition, especially sapphire-bearing ones, are uncommon. Petrogenesis of this rare sapphire-bearing syenitoid pegmatite is virtually unknown because similar pegmatites have not been reported from Iran and are very rare elsewhere in the world. Sapphire is reported from diverse lithologies, but in pegmatites it is not a common mineral. Therefore, this study focuses on a sapphire-bearing pegmatite within the SSZ, which is of particular interest because of its unique geochemical and petrological characteristics and also its potential as a key for gemstone exploration in this zone.

In recent decades, geologists have attributed the magmatic activities to the geotectonic environment of the regions. The ore composition and type of ore body as well as mineralogy are related to the geological environment and geodynamic setting of the pegmatite. In this regard, granitoids and related granitic pegmatites are significant in the interpretation of ancient geodynamic regimes. Also, type of host rock lithology, shape and structures, chemical and mineralogical qualifiers are important for the applied and genetic economic geological classification of pegmatites. On the other hand, the link between geology and mineralogy of pegmatites can be made by studying the chemical composition, mineral assemblage and structural geology of these rocks (Dill, 2015, 2016).

Granitoids and related granitic pegmatites occur in various geodynamic settings from anorogenic to orogenic systems. Northwest of the SSZ, a spectrum of granitoid types is present in plutonic bodies (i.e. I-, S-, M- and A-type granitoids). In the majority of the plutonic bodies of the SSZ, substantial parts are granitoids, but small volumes of granitic pegmatites also occur (see Section 4.c below).

Many recent studies on the petrogenesis and geochronology of plutonic rocks of the Hamedan region exist (e.g. Shahbazi *et al.* 2010; Mahmoudi *et al.* 2011; Chiu *et al.* 2013; Sepahi *et al.* 2018; Yang *et al.* 2018; Zhang *et al.* 2018a, b), but SBPs have not been the target of these earlier research efforts (i.e. geochronology and zircon geochemistry of these rocks have not been studied earlier). The whole-rock geochemical compositions of the SBPs are unique (Table 1), plotting in fields quite different on geochemical compositional discrimination diagrams so that selecting a single name for them is very difficult, although they resemble some syenitic rocks in their mineral and chemical compositions.

The study of pegmatites reveals further information about the geological evolution of the region and the SSZ as an important tectono-stratigraphic unit of the Zagros orogen, Iran. In spite of smaller volumes of granitic pegmatites in contrast to other granitoid rocks, they can yield significant geological, petrological and geodynamic information about the studied region. Most previously investigated pegmatites that occur in the northwest of the SSZ are mildly peraluminous to metaluminous (e.g. S Salami, unpub. PhD, Bu-Ali Sina University, Hamedan, Iran, 2017), but our study reveals that SBPs of the region are extremely peraluminous without any distinct genetic relationship with other pegmatites and host granitoids.

Although most pegmatites commonly have simple quartzofeldspathic mineralogy, they have diverse minor minerals and in many places also contain minerals suitable for U–Pb geochronology, such as monazite and zircon. A number of characteristics of zircon, such as high U–Th concentrations, its occurrence in various lithologies, its refractory nature in metamorphic and magmatic conditions and its resistance to physical and chemical weathering,

make zircon most suitable for robust geochronology and thus a good tool for interpreting diverse earth processes (e.g. Kirkland *et al.* 2015; Gao *et al.* 2016). Also, in recent years geochemical compositions of zircon have been used for fractionation studies to estimate redox conditions of magmas (e.g. Ballard *et al.* 2002; Shen *et al.* 2015) for geochemical exploration. Several methods of zircon geochronology exist, but in this study, zircon geochronology and geochemistry have been performed on selected polished thin-sections of three pegmatite samples by laser ablation inductively coupled plasma mass spectrometry (LA-ICP-MS) (Table 2). In this paper, U–Pb zircon geochronology has been performed on the sapphire-bearing syenitoid pegmatites in order to compare their ages with those of other previously dated pegmatites and associated host granitoids. Also, whole-rock litho-geochemistry and zircon geochemistry are presented to help formulate a petrogenetic interpretation, as well as add further insight into the geological evolution of the Hamedan region as a significant part of the SSZ.

2. Geological setting

The Zagros orogen is midway in the Alpine–Himalayan orogenic system and extends from NW to SE Iran. It includes three parallel belts (from SW to NE): the Zagros fold-and-thrust belt, the Sanandaj–Sirjan zone (SSZ) and the Urumieh–Dokhtar Magmatic Belt (Arc) (Alavi, 1994, 2004). The SSZ (including the study area) is a NW–SE-trending plutono-metamorphic belt that is 150–200 km wide and more than 1500 km long, is nearly parallel to the Zagros main thrust fault and has low- to high-grade metamorphic rocks intruded by mafic (gabbroic) to felsic (granitic) plutons. The tectono-magmatic history of the SSZ is related to the opening and closure of the Neo-Tethys Ocean from the Permo-Triassic to Cenozoic time interval. The SSZ has been considered as a typical active continental margin with significant magmatism in the Mesozoic (e.g. Takin, 1972; Ghasemi & Talbot, 2006; Mehdipour-Ghazi & Moazzen, 2015; Hassanzadeh & Wernicke, 2016). This magmatic arc was formed by subduction of Neo-Tethyan oceanic crust beneath the central Iranian micro-continent south of the Eurasian supercontinent. In this tectono-magmatic unit, several plutonic complexes (Fig. 1) crop out and their major lithologies are granitic in composition. The Alvand plutonic complex, comprising various plutonic rocks from mafic to felsic, occurs in the Hamedan region (Fig. 2). This plutonic complex (so-called Alvand Batholith) crops out over an area of nearly 400 km² and consists of a variety of plutonic rocks, such as olivine gabbro, gabbro, norite, gabbro-norite, diorite, tonalite, granodiorite, monzogranite, syenogranite, and leucocratic granitoids intruded by aplitic to pegmatitic dykes. Granitoids and associated pegmatites/aplites of this complex are significant for the interpretation of the geological evolution of the region and adjacent areas in the SSZ (e.g. Sepahi *et al.* 2018).

The various rocks of the Alvand plutonic complex (Hamedan) have been previously dated. Valizadeh & Cantagrel (1975) reported 63–90 Ma ages for these rocks, based on a ⁴⁰K–³⁹Ar geochronological method on their micas, including 89.1 ± 3.0 Ma for the norites, 63.8 ± 3.0 Ma for the porphyritic granites and ~83 Ma for the pegmatites. J Braud (unpub. PhD, Univ. Paris, 1987) determined a similar age of 64 ± 2 Ma for the granites, based on the ⁴⁰K–³⁹Ar method. According to the K–Ar method, with ages determined by Baharifar *et al.* (2004) using amphibole, biotite and muscovite, the Alvand plutonic complex ages are from 70 to 135 Ma, with 81.8 ± 1.9 Ma for the porphyritic granites, 74.7 ± 1.8 Ma for the pegmatites (in the Zamanabad area), 73.2 ± 3.1 Ma for the quartz

Table 1. Whole-rock chemical compositions of the studied granitoids and pegmatite samples

Sample	SMV-131	SMV-131b	SMV-1	ME-108	M-4	SMV-182	ME-415	M-1	ME-414	ME-429	M-8	ME-417	SMV-197	SMV-206
	Sapphire-bearing pegmatites							Granitoids						
Oxides (wt %)														
SiO ₂	51.79	52.11	54.15	64.66	64.80	64.99	66.37	66.40	66.96	66.99	67.70	68.05	68.56	68.63
TiO ₂	0.04	0.04	0.04	0.35	0.66	0.80	0.65	0.86	0.71	0.77	0.63	0.58	0.52	0.34
Al ₂ O ₃	33.42	33.34	31.63	17.96	15.45	15.57	16.10	14.95	15.82	15.40	14.25	15.39	15.18	15.40
Fe ₂ O ₃ *	1.43	1.66	1.20	3.99	6.81	6.39	5.25	7.31	5.38	5.44	4.85	4.60	4.01	3.84
MnO	0.02	0.03	0.02	0.05	0.14	0.08	0.09	0.13	0.09	0.09	0.06	0.08	0.06	0.08
MgO	0.02	0.02	0.02	0.74	1.19	1.43	1.21	1.37	1.16	1.30	0.94	0.95	0.81	0.44
CaO	0.23	0.21	0.51	2.60	0.92	2.71	1.77	2.21	2.46	2.10	1.91	1.76	1.60	1.52
Na ₂ O	3.86	3.82	4.69	3.61	3.20	3.13	2.70	3.66	3.76	2.26	3.16	2.95	2.84	3.79
K ₂ O	7.59	7.64	6.70	4.80	5.19	3.71	4.38	2.57	2.76	4.34	3.92	4.63	5.14	5.16
P ₂ O ₅	nd	nd	nd	0.25	0.20	0.19	0.21	0.32	0.15	0.18	0.14	0.21	0.21	0.09
LOI	1.50	1.00	1.00	0.70	1.23	0.80	1.10	0.95	0.60	0.90	0.64	0.60	0.90	0.50
Total	99.91	99.92	99.91	99.84	99.82	99.85	99.86	100.75	99.84	99.86	98.23	99.85	99.87	99.83
Trace elements (ppm)														
Rb	335	328	275	152	448	175	190	357	182	141	205	209	210	264
Cs	9	7	7	5	68	12	13	40	19	7	9	15	12	18
Sr	28	14	29	353	50	197	140	61	134	173	77	141	144	162
Ba	51	31	33	1098	160	236	427	68	170	527	155	367	502	280
Sc	nd	nd	nd	7	nd	11	11	nd	11	13	nd	9	8	5
Co	1	1	1	8	nd	12	10	nd	9	11	nd	9	7	4
Ga	90	95	74	20	26	22	22	25	22	18	21	20	19	19
Y	2	2	1	23	33	15	30	37	27	28	32	22	19	33
Zr	11	10	16	287	180	203	250	173	382	230	207	214	210	272
Nb	31	41	24	18	27	32	19	40	22	17	28	18	17	27
Sn	18	18	13	2	16	6	6	12	6	5	6	6	7	6
Hf	1	1	1	8	5	5	7	5	10	6	6	6	6	6
Ta	2	3	1	1	2	2	2	3	2	1	1	2	1	2
W	4	3	2	1	2	2	3	2	1	2	2	2	3	2
Th	2	3	2	33	18	14	16	21	19	17	29	15	14	27
U	2	2	1	3	3	2	3	3	3	2	2	2	2	3
La	8.8	6.9	13.9	83.6	35.6	44.5	42.4	38.1	42.5	42.9	47.4	39.6	38.3	68.5
Ce	9.3	9.5	16.8	163.6	67.2	83.8	86.0	72.2	84.9	88.9	90.4	80.4	73.9	122.1
Pr	0.7	0.8	1.3	16.9	7.6	9.1	9.6	8.1	8.9	9.4	10.2	8.6	7.8	11.9
Nd	1.8	2.2	3.7	60.8	28.1	32.8	36.3	29.0	32.7	35.3	35.2	33.7	28.5	41.3
Sm	0.17	0.21	0.40	10.62	5.98	6.48	7.43	6.17	6.21	6.57	7.58	6.59	5.70	7.21
Eu	0.12	0.07	0.13	1.79	0.48	1.07	1.22	0.40	1.02	1.61	0.68	1.09	1.08	0.79
Gd	0.19	0.27	0.31	8.24	5.72	5.50	6.54	5.88	5.80	6.03	6.84	5.87	5.08	6.47
Tb	0.03	0.05	0.04	1.07	0.93	0.72	0.98	1.10	0.89	0.89	1.09	0.85	0.74	1.01
Dy	0.26	0.30	0.27	5.10	5.79	3.34	5.58	6.97	4.91	5.12	6.45	4.73	3.82	5.75
Ho	0.06	0.07	0.04	0.96	1.23	0.55	1.05	1.36	0.99	1.02	1.20	0.86	0.70	1.19
Er	0.17	0.28	0.12	2.27	3.55	1.51	3.21	3.88	2.89	2.89	3.41	2.34	1.93	3.36
Tm	0.03	0.04	0.02	0.32	0.53	0.20	0.42	0.54	0.42	0.46	0.47	0.33	0.26	0.47

(Continued)

Table 1. (Continued)

Sample	SMV-131	SMV-131b	SMV-1	ME-108	M-4	SMV-182	ME-415	M-1	ME-414	ME-429	M-8	ME-417	SMV-197	SMV-206
Yb	0.20	0.28	0.11	2.18	3.61	1.24	2.86	3.52	2.76	2.96	2.72	2.10	1.74	3.13
Lu	0.03	0.04	nd	0.31	0.49	0.19	0.42	0.47	0.44	0.41	0.41	0.30	0.27	0.41
Eu/Eu*	1.90	0.84	1.01	0.52	0.23	0.49	0.48	0.18	0.47	0.71	0.26	0.49	0.56	0.32
ΣREE	21	20	37	357	166	190	204	177	195	204	214	187	169	273
ΣHREE	1	1	1	12	16	7	14	17	13	14	16	11	9	15
ΣLREE	20	19	36	345	150	183	189	159	182	190	198	176	160	258
T _{Zircon} (°C)	615	614	635	834	802	802	841	795	870	831	802	818	815	828
T _{Monazite} (°C)	739	735	770	869	807	801	845	802	816	839	814	818	807	827
	ME-418	RMK-C-7	RMK-D-51	RMK-B	SMV-194	RMK-B-5	SMV-190	RMK-A-1	SMV-175	SMV-204	RMK-D-5	ME-6	ME-413	SMV-195
Sample	Granitoids							Other pegmatites						
Oxides (wt %)														
SiO ₂	69.04	69.80	70.60	71.40	71.47	71.60	73.13	73.30	73.81	73.96	74.00	74.81	75.41	75.55
TiO ₂	0.63	0.34	0.40	0.45	0.14	0.36	0.14	0.37	0.01	0.09	0.41	0.01	0.01	0.07
Al ₂ O ₃	15.08	15.35	15.20	14.65	15.10	14.85	14.37	13.95	13.82	13.98	13.70	13.93	14.58	13.54
Fe ₂ O ₃ *	4.59	2.79	3.79	3.48	1.75	2.93	1.24	3.02	0.77	1.73	3.13	0.99	0.90	1.15
MnO	0.06	0.04	0.08	0.05	0.03	0.06	0.02	0.06	0.02	0.04	0.05	0.05	0.08	0.06
MgO	0.97	0.52	0.73	0.71	0.24	0.59	0.19	0.53	0.04	0.16	0.63	0.06	0.05	0.06
CaO	2.44	1.45	1.04	1.19	1.18	1.01	0.84	1.16	0.18	0.84	0.86	1.08	0.40	0.33
Na ₂ O	3.73	3.30	3.19	3.09	3.63	3.04	2.37	3.10	2.03	3.09	2.95	2.74	4.23	3.87
K ₂ O	2.81	5.33	5.29	4.94	5.80	5.55	7.27	5.15	8.82	5.43	4.38	5.95	3.64	4.85
P ₂ O ₅	0.14	0.10	0.13	0.07	0.12	0.14	0.11	0.12	0.11	0.15	0.08	0.05	0.28	0.14
LOI	0.40	0.67	1.10	0.90	0.40	0.85	0.20	0.50	0.30	0.40	0.93	0.20	0.40	0.30
Total	99.87	99.75	101.59	100.97	99.90	101.03	99.93	101.29	99.92	99.91	101.16	99.95	99.97	99.94
Trace elements (ppm)														
Rb	173	182	246	187	201	237	173	255	221	192	166	118	242	228
Cs	7	7	19	10	10	16	9	18	6	14	7	1	1	11
Sr	87	118	84	124	106	86	154	83	109	97	135	274	29	26
Ba	94	412	292	381	327	297	381	263	222	193	302	857.00	33.00	34.00
Sc	8	nd	nd	nd	2	nd	2	nd	1	3	nd	2	1	5
Co	9	nd	nd	nd	2	nd	2	nd	1	2	nd	1	1	1
Ga	23	20	20	20	15	18	11	20	9	13	18	12	13	14
Y	24	27	28	29	11	27	10	30	8	19	31	12	3	10
Zr	238	187	206	216	89	174	23	158	15	23	219	75	17	32
Nb	18	16	26	20	6	24	6	22	1	6	18	1	2	14
Sn	3	4	7	5	7	6	5	8	5	7	4	nd	9	3
Hf	6	5	6	6	3	5	1	5	1	1	6	3	1	1
Ta	1	1	2	1	1	2	1	2	1	2	1	nd	1	5
W	nd	1	2	2	2	1	1	6	nd	2	2	nd	1	7
Th	22	27	30	29	9	27	5	25	1	3	26	4	1	2
U	3	2	3	2	1	2	1	3	1	2	2	1	1	1
La	39.2	46.4	48.7	53.5	19.6	40.5	12.3	37.2	2.2	8.0	46.1	8.3	1.3	4.7
Ce	83.7	88.2	91.1	102.0	37.4	77.2	21.2	69.3	3.2	15.4	88.6	14.0	2.6	8.9
Pr	8.96	9.73	10.05	11.50	3.79	8.04	2.15	7.83	0.27	1.66	9.65	1.51	0.32	1.01

(Continued)

Table 1. (Continued)

Sample	ME-418	RMK-C-7	RMK-D-51	RMK-B	SMV-194	RMK-B-5	SMV-190	RMK-A-1	SMV-175	SMV-204	RMK-D-5	ME-6	ME-413	SMV-195
	Granitoids								Other pegmatites					
Nd	32.8	34.5	34.0	39.5	14.1	28.0	7.9	26.5	0.8	6.4	33.8	5.9	1.2	3.5
Sm	7.36	6.84	6.46	7.57	2.83	5.52	1.42	4.94	0.23	1.56	6.71	1.30	0.31	0.78
Eu	0.70	0.95	0.70	0.99	0.78	0.70	0.97	0.69	0.67	0.69	0.85	1.20	nd	0.16
Gd	6.41	5.96	5.72	6.71	2.59	4.99	1.54	4.86	0.40	1.91	5.93	1.34	0.38	0.90
Tb	0.96	0.91	0.90	0.99	0.42	0.80	0.26	0.85	0.11	0.43	0.94	0.24	0.08	0.18
Dy	4.85	5.42	5.42	5.84	2.17	4.89	1.65	5.18	1.07	2.94	5.79	1.79	0.52	1.49
Ho	0.85	1.02	0.98	1.04	0.41	0.94	0.31	1.11	0.31	0.67	1.11	0.45	0.08	0.37
Er	2.31	2.74	2.98	2.76	1.02	2.88	0.93	3.15	1.12	2.35	3.26	1.68	0.23	1.38
Tm	0.30	0.36	0.42	0.40	0.16	0.44	0.13	0.47	0.20	0.39	0.44	0.28	0.04	0.29
Yb	2.14	2.51	2.74	2.40	0.95	2.91	0.92	3.10	1.50	2.79	3.01	2.17	0.34	2.34
Lu	0.34	0.34	0.44	0.37	0.14	0.41	0.11	0.46	0.25	0.44	0.42	0.33	0.05	0.38
Eu/Eu*	0.28	0.41	0.32	0.38	0.80	0.37	1.86	0.39	6.26	1.14	0.37	2.57	nd	0.54
ΣREE	190	205	210	235	86	178	51	165	12	45	206	40	7	26
ΣHREE	11	13	13	13	5	13	4	14	4	10	14	7	1	6
ΣLREE	179	192	196	221	81	164	47	151	8	35	192	33	6	19
T _{zircon} (°C)	822	802	817	821	735	801	644	789	614	648	832	729	635	669
T _{Monazite} (°C)	807	816	831	841	734	813	702	794	579	689	843	679	598	650

*All Fe is assumed to be Fe³⁺. LOI = loss on ignition; nd = not detected.

Table 2. LA-ICP-MS data of analysed zircon grains used for U–Pb dating

Spot	Concentrations (ppm)					Isotopic ratios and errors (2σ)								Age (Ma)			
	U (ppm)	Th (ppm)	Th/U	²⁰⁷ Pb/ ²³⁵ U	2σ	²⁰⁶ Pb/ ²³⁸ U	2σ	Err. corr	²³⁸ U/ ²⁰⁶ Pb	2σ	²⁰⁷ Pb/ ²⁰⁶ Pb	2σ	Err. corr	²⁰⁷ Pb/ ²³⁵ U	2σ	²⁰⁶ Pb/ ²³⁸ U	2σ
SMV-1-1	773	360	0.47	0.182	0.004	0.026	0.000	0.219	38.02	0.49	0.050	0.001	0.12	169	3	167	2
SMV-1-2	440	174	0.39	0.182	0.005	0.026	0.000	0.099	38.58	0.55	0.051	0.001	0.24	169	4	165	2
SMV-1-3	709	88	0.12	0.178	0.004	0.026	0.000	0.163	38.31	0.50	0.050	0.001	0.16	167	3	166	2
SMV-1-4	2580	3753	1.45	0.186	0.002	0.027	0.000	0.181	37.41	0.48	0.051	0.001	0.42	173	2	170	2
SMV-1-5	2164	3281	1.51	0.215	0.003	0.026	0.000	0.095	38.37	0.50	0.060	0.001	0.37	197	3	166	2
SMV-1-6	1059	1305	1.23	0.197	0.005	0.026	0.000	0.417	38.64	0.60	0.055	0.001	nd	182	4	165	3
SMV-1-7	842	238	0.28	0.187	0.035	0.028	0.001	0.656	32.78	0.54	0.114	0.002	0.24	167	30	178	4
SMV-1-8	2620	4800	1.82	0.210	0.005	0.026	0.000	0.706	38.97	0.67	0.059	0.002	nd	193	5	163	3
SMV-1-9	2370	3963	1.67	0.180	0.003	0.026	0.000	0.212	37.79	0.49	0.049	0.001	0.24	168	2	168	2
SMV-1-10	1980	3650	1.85	0.206	0.004	0.026	0.000	0.556	37.99	0.55	0.057	0.001	nd	190	3	168	2
SMV-1-11	1309	321	0.25	0.180	0.003	0.027	0.000	0.174	37.62	0.48	0.049	0.001	0.24	168	3	169	2
SMV-1-12	1419	2169	1.54	0.208	0.005	0.027	0.000	0.270	36.78	0.53	0.055	0.001	0.14	192	4	173	2
SMV-1-14	875	131	0.15	0.205	0.005	0.027	0.000	0.415	37.06	0.55	0.055	0.001	nd	189	4	172	3
SMV-1-15	1155	460	0.40	0.193	0.004	0.027	0.000	0.118	37.69	0.48	0.053	0.001	0.28	179	3	169	2
SMV-1-16	563	277	0.49	0.182	0.005	0.026	0.000	0.206	38.79	0.56	0.051	0.001	0.15	170	4	164	2
SMV-1-17	842	170	0.20	0.216	0.006	0.027	0.000	0.273	36.54	0.53	0.057	0.002	0.08	198	5	174	3
SMV-1-18	681	83	0.12	0.162	0.071	0.026	0.001	0.875	28.29	0.39	0.277	0.004	0.40	120	69	165	6
SMV-1-19	674	398	0.59	0.244	0.007	0.027	0.000	0.321	36.76	0.53	0.065	0.002	0.02	222	6	173	2

(Continued)

Table 2. (Continued)

Spot	Concentrations (ppm)			Isotopic ratios and errors (2σ)										Age (Ma)			
	U (ppm)	Th (ppm)	Th/U	²⁰⁷ Pb/ ²³⁵ U	2σ	²⁰⁶ Pb/ ²³⁸ U	2σ	Err. corr	²³⁸ U/ ²⁰⁶ Pb	2σ	²⁰⁷ Pb/ ²⁰⁶ Pb	2σ	Err. corr	²⁰⁷ Pb/ ²³⁵ U	2σ	²⁰⁶ Pb/ ²³⁸ U	2σ
SMV-1-20	1078	820	0.76	0.233	0.005	0.026	0.000	0.197	38.28	0.59	0.065	0.001	0.22	212	4	166	3
SMV-1-21	530	517	0.97	0.264	0.008	0.026	0.000	0.145	38.33	0.65	0.074	0.002	0.23	238	7	166	3
SMV-1-22	95	31	0.32	0.301	0.017	0.029	0.001	0.167	34.09	0.78	0.075	0.004	0.46	267	13	186	4
SMV-1-23	620	440	0.71	0.390	0.009	0.029	0.000	0.143	35.05	0.50	0.099	0.002	0.27	334	7	181	3
SMV-1-24	925	93	0.10	0.174	0.040	0.026	0.001	0.745	35.64	0.57	0.123	0.002	0.40	160	36	163	4
SMV-1-25	1090	1020	0.93	0.213	0.005	0.027	0.000	0.205	36.71	0.53	0.057	0.001	0.23	196	4	173	2
SMV-1-26	4720	11 500	2.44	0.160	0.008	0.024	0.000	0.545	41.36	0.68	0.057	0.001	0.21	151	7	152	3
SMV-1-27	291	59	0.20	0.490	0.250	0.037	0.002	0.813	12.99	0.27	0.565	0.008	nd	410	180	231	14
SMV-1-28	284	329	1.16	0.170	0.240	0.030	0.002	0.910	22.93	0.53	0.311	0.009	0.45	90	230	193	15
SMV-1-29	2224	3309	1.49	0.156	0.029	0.026	0.000	0.537	33.98	0.57	0.142	0.002	nd	142	26	165	3
SMV-1-30	2167	2097	0.97	0.167	0.014	0.025	0.000	0.576	38.48	0.53	0.074	0.002	0.23	156	12	160	3
SMV-131-1	1652	2514	1.51	0.196	0.005	0.026	0.000	0.373	38.70	0.66	0.055	0.001	0.14	181	4	164	3
SMV-131-2	1108	53	0.05	0.200	0.004	0.026	0.000	0.355	38.21	0.50	0.055	0.001	0.02	185	3	167	2
SMV-131-3	479	115	0.24	0.190	0.012	0.026	0.001	0.120	38.87	0.89	0.054	0.004	0.42	176	10	164	4
SMV-131-4	4675	464	0.10	0.180	0.002	0.026	0.000	0.358	38.28	0.47	0.050	0.000	0.25	168	2	166	2
SMV-131-5	499	222	0.44	0.178	0.005	0.025	0.000	0.041	39.23	0.55	0.051	0.001	0.27	166	4	162	2
SMV-131-6	445	202	0.45	0.185	0.005	0.026	0.000	0.016	39.11	0.58	0.052	0.002	0.33	172	5	163	2
SMV-131-7	2123	4790	2.27	0.193	0.002	0.027	0.000	0.145	37.65	0.47	0.053	0.001	0.36	179	2	169	2
SMV-131-8	1534	2051	1.33	0.187	0.028	0.026	0.001	0.592	36.01	0.70	0.102	0.002	nd	171	25	166	4
SMV-131-9	440	138	0.31	0.253	0.007	0.027	0.000	0.211	37.72	0.57	0.069	0.002	0.16	229	6	169	3
SMV-131-10	947	904	0.95	0.179	0.003	0.026	0.000	0.133	38.24	0.50	0.050	0.001	0.25	167	3	166	2
SMV-131-11	12 117	3482	0.29	0.179	0.012	0.026	0.000	0.375	35.05	0.44	0.121	0.001	0.27	167	10	166	2
SMV-131-12	823	223	0.27	0.178	0.004	0.026	0.000	0.175	38.61	0.52	0.050	0.001	0.21	166	3	165	2
SMV-131-13	2833	301	0.11	0.177	0.003	0.026	0.000	0.429	38.93	0.52	0.050	0.001	0.01	166	3	164	2
SMV-131-14	1113	308	0.28	0.250	0.010	0.027	0.000	0.478	37.61	0.59	0.067	0.002	nd	226	8	169	3
SMV-131-15	3693	220	0.06	0.185	0.002	0.027	0.000	0.372	37.61	0.48	0.051	0.001	0.25	173	2	169	2
SMV-131-16	1869	3233	1.79	0.180	0.003	0.026	0.000	0.184	38.49	0.49	0.050	0.001	0.29	168	2	165	2
SMV-131-17	812	179	0.22	0.177	0.004	0.025	0.000	0.131	39.34	0.53	0.050	0.001	0.24	165	3	162	2
SMV-131-18	6000	979	0.16	0.190	0.013	0.027	0.000	0.392	33.06	0.44	0.128	0.001	0.01	176	11	174	2
SMV-131-19	594	222	0.37	0.175	0.005	0.025	0.000	0.068	39.48	0.58	0.050	0.001	0.29	164	4	161	2
SMV-131-20	296	90	0.30	0.188	0.009	0.026	0.000	0.191	38.46	0.72	0.053	0.003	0.48	175	8	165	3
SMV-131-21	1604	934	0.58	0.190	0.005	0.027	0.000	0.251	37.34	0.61	0.052	0.001	0.23	176	4	170	3
SMV-131-22	445	174	0.39	0.365	0.009	0.028	0.000	0.119	36.13	0.55	0.096	0.002	0.32	315	7	176	3
SMV-131-23	1099	1000	0.90	0.195	0.035	0.026	0.001	0.748	34.63	0.48	0.139	0.002	0.31	175	29	164	4
SMV-131b-1	1534	592	0.39	0.190	0.029	0.027	0.001	0.736	32.01	0.45	0.160	0.002	0.06	170	25	173	3
SMV-131b-2	520	159	0.31	0.174	0.004	0.026	0.000	0.064	38.77	0.54	0.049	0.001	0.43	163	3	164	2
SMV-131b-3	751	146	0.18	0.179	0.004	0.025	0.000	0.172	39.49	0.56	0.052	0.001	0.19	167	3	161	2
SMV-131b-4	1951	3024	1.54	0.190	0.003	0.026	0.000	0.241	38.96	0.49	0.054	0.001	0.19	177	3	163	2
SMV-131b-5	1006	162	0.16	0.182	0.004	0.027	0.000	0.026	37.72	0.50	0.050	0.001	0.31	170	3	169	2
SMV-131b-6	3740	570	0.15	0.192	0.002	0.028	0.000	0.217	36.17	0.44	0.050	0.001	0.34	178	2	176	2
SMV-131b-7	884	640	0.72	0.144	0.050	0.026	0.001	0.766	34.82	0.52	0.126	0.003	0.08	136	46	165	5
SMV-131b-8	451	344	0.76	0.176	0.006	0.025	0.000	0.202	39.46	0.62	0.050	0.002	0.17	164	5	161	3

(Continued)

Table 2. (Continued)

Spot	Concentrations (ppm)				Isotopic ratios and errors (2σ)							Age (Ma)					
	U (ppm)	Th (ppm)	Th/U	²⁰⁷ Pb/ ²³⁵ U	2σ	²⁰⁶ Pb/ ²³⁸ U	2σ	Err. corr	²³⁸ U/ ²⁰⁶ Pb	2σ	²⁰⁷ Pb/ ²⁰⁶ Pb	2σ	Err. corr	²⁰⁷ Pb/ ²³⁵ U	2σ	²⁰⁶ Pb/ ²³⁸ U	2σ
SMV-131b-9	570	147	0.26	0.180	0.005	0.026	0.000	0.183	38.70	0.57	0.050	0.001	0.16	167	5	165	2
SMV-131b-10	1071	690	0.65	0.204	0.006	0.026	0.000	0.275	38.97	0.58	0.058	0.002	0.00	188	5	163	2
SMV-131b-11	3800	453	0.12	0.186	0.003	0.027	0.000	0.494	36.98	0.49	0.050	0.001	0.19	174	2	172	2
SMV-131b-12	2376	204	0.09	0.189	0.003	0.026	0.000	0.267	38.02	0.52	0.052	0.001	0.25	175	3	167	2
SMV-131b-13	664	234	0.35	0.187	0.005	0.026	0.000	0.091	37.86	0.57	0.052	0.001	0.23	174	4	168	3
SMV-131b-14	325	90	0.28	0.320	0.010	0.028	0.000	0.055	36.25	0.60	0.084	0.003	0.43	282	7	175	3
SMV-131b-15	363	117	0.32	0.554	0.019	0.028	0.000	0.509	35.11	0.58	0.141	0.004	nd	446	12	181	3
SMV-131b-16	1832	3087	1.69	0.176	0.003	0.026	0.000	0.046	38.88	0.48	0.050	0.001	0.41	164	2	164	2

nd = not detected.

diorites and 135.2 ± 3.1 Ma for the diorites. Valizadeh & Cantagrel (1975) determined 68–89 Ma ages for the complex rocks using the ⁸⁷Rb–⁸⁶Sr isochron method, including 78–89 Ma for the norites, 68 ± 2 Ma for the porphyritic granites and 104.3 ± 3.0 Ma for the pegmatites. Recent U–Pb data give different results that indicated a Middle–Late Jurassic (150–170 Ma) age for plutonic rocks and aplitic–pegmatitic rocks (e.g. Shahbazi *et al.* 2010; Mahmoudi *et al.* 2011; Chiu *et al.* 2013; Sepahi *et al.* 2018; Yang *et al.* 2018; Zhang *et al.* 2018a, b).

Petrological properties of aplitic–pegmatitic dykes, which cross-cut the plutonic and metamorphic rocks of the Hamedan region, resemble lithium–caesium–tantalum (LCT) pegmatites. Common LCT pegmatitic rocks of the region belong to muscovite (MS) and muscovite–rare-element (MSREL) classes (cf. Cerný & Ercit, 2005). They commonly contain quartz, feldspar and mica, with minor tourmaline, garnet, beryl and spodumene (see Sepahi *et al.* 2018). Also, regional and contact metamorphic rocks of the region are diverse, varying from low- to high-grade. They are mainly metapelitic in composition, but interlayers of metapsammites, metacarbonates, metabasites and calc-silicates occur as well. The metamorphic age of the metamorphic rocks is Early–Middle Jurassic (around 160–180 Ma; Sepahi *et al.* 2019). The main lithologies include slate, phyllite, mica schist, garnet–mica schist, garnet–andalusite–mica schist, garnet–andalusite–sillimanite–mica schist, garnet–staurolite–mica schist, Al₂SiO₅-bearing and cordierite-bearing migmatite, amphibolite, andalusite–cordierite hornfels, and cordierite–K-feldspar hornfels. Metamorphism is low pressure / high temperature (andalusite–sillimanite geotherm; Abukuma or Buchan type), although in some places moderate-pressure metamorphism (kyanite geotherm; Barrovian type) is recorded by the development of index minerals such as kyanite (e.g. Sepahi *et al.* 2004, 2009).

3. Results

3.a. Sampling and technical details

One part of this study is to ascertain the age of syenitoid pegmatites in the Hamedan region, using zircon U–Pb geochronology. For this purpose, 150 samples were collected from fresh lithologies of outcrops (63 pegmatites, 53 granitoids and 34 metamorphic rocks). Eighty thin-sections and ten polished thin-sections were prepared and studied with an optical microscope. Ultimately, three samples from SBPs with polished thin-sections were chosen for zircon U–Pb LA-ICP-MS geochronology and zircon trace element

studies. Fusion ICP-MS and ICP emission spectrometry (ICP-ES) analyses of large whole rock samples were done. Major elements analyses were measured using ICP-ES with the lithium metaborate/tetraborate fusion method in Acme Analytical Laboratories (Acme Labs) in Canada. The detection limits for major elements varied from 0.01 to 0.1 wt %. Loss on ignition (LOI) was determined on the dried samples heated at 1000 °C. For trace and rare earth element (REE) analyses, 0.2 g samples were mixed with 1.5 g LiBO₂ and dissolved in 100 ml 5% HNO₃. Trace element and REE analyses were completed with an ICP-MS in Acme Labs in which detection limits range from 0.1 to 10 ppm for trace elements and from 0.01 to 0.5 ppm for REE.

For X-ray fluorescence (XRF) mapping of polished thin-sections, we used a Bruker benchtop M4 Tornado μ-XRF instrument (see Flude *et al.* 2017). This system has a Rh X-ray tube, dual silicon-drifted detectors (SDDs), and polycapillary optics giving an X-ray beam with a nominal spot size of 20 μm and similar steps allowing for element mapping of a full polished thin-section at a similar pixel resolution of roughly 20 μm. Detailed imaging of zircon was carried out using 5 μm increment steps with spot size of 20 μm (resolution ~10 μm) and much longer integration times (20 ms) per 20 μm spot. All maps were collected at 50 kV and 400 uA.

U–Pb LA ICP-MS geochronology of 30 μm thick polished thin-sections was conducted following standard procedures. Optical identification of accessory minerals by the polarizing microscope was followed by detailed micro-XRF maps (noted above) showing the size and distribution of zircon. In this study, an Australian Scientific Instruments (formerly Resonetics) M-50-LR193 nm ArF excimer laser ablation system coupled to Agilent 7700x quadrupole ICP-MS was used for U–Pb geochronology on polished thin-sections (see McFarlane & Luo, 2012). Crater diameter was 24 μm for zircon dating. Data reduction was done using Iolite™ and VizualAge™. Data output and assessment of accuracy were done using quality-control standards (e.g. Plesovice zircon). Concordia diagrams were drawn by ISOPLOT/EX 3.75 software (Ludwig, 2003). LA ICP-MS for dating and trace element geochemistry was done on zircon grains from three selected polished thin-sections with a total of 69 analysed spots: SMV-1 ($n = 30$), SMV-131 ($n = 23$) and SMV-131-b ($n = 16$).

3.b. Field observations

Pegmatites and aplites of the Hamedan region occur in the interior, marginal and exterior areas of the plutonic bodies. Where they

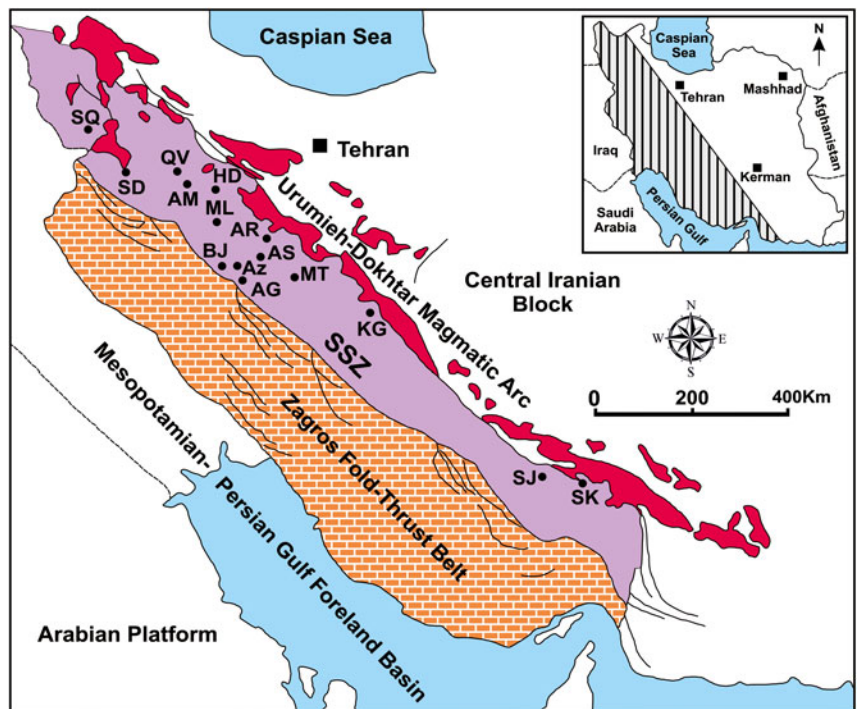


Fig. 1. (Colour online) Localities of major plutonic bodies in the Sanandaj–Sirjan zone, Zagros orogen, Iran (modified after Moazzen *et al.* 2004 and Sepahi & Athari, 2006). SQ: Saqqez, SD: Sanandaj, QV: Qorveh, AM: Almogholagh, HD: Hamedan (Alvand), ML: Malayer, BZ: Boroujerd, AR: Arak, AS: Astaneh, AZ: Azna, AG: Aligoudarz, MT: Muteh (Hasanrobat), KG: Kolah-Ghazi, SJ: Sirjan and SK: Siah Kouh.

exist exterior to the plutons, their host rocks are schists and hornfels of the Hamedan metamorphic complex (e.g. Sepahi *et al.* 2018). Pegmatites of the region occur as pods and dykes that intrude the various plutonic and metamorphic rocks. Widths of dykes are a few centimetres to more than 3 m. They are closely associated with aplites in single dykes or as separate pegmatites without aplites. Where they occur in composite dykes, the aplites commonly occur in the marginal zone (Fig. 3a), but in some places the aplites layers alternate with pegmatite layers in a single dyke (Fig. 3b). Layered aplites occur in some outcrops. Where hosts of pegmatites are metamorphic rocks, they occur nearly parallel to the schistosity of the host rocks. Tourmaline-bearing pegmatites are the most frequent variety of pegmatites in the region (Fig. 3c). SBPs are rare (Fig. 3d), but occur south of Khakou (south of Hamedan). There is no evidence of silica-deficient rock units, such as ultramafites and meta-carbonates, in accidental and/or tectonic contact with the sapphire-bearing pegmatitic dyke (i.e. granitoids and meta-pelitic hornfels occur adjacent to the dyke).

3.c. Petrography

Various types of igneous and metamorphic rocks crop out in the region. The igneous rocks are mostly granitoids, including quartz monzonite, granodiorite, monzogranite, syenogranite, and pegmatite and aplitite. Also, a small volume of leucocratic granitoids occur in the region. Gabbroid and dioritic rocks also occur in the region (Sepahi, 2008; Sepahi *et al.* 2018). The metamorphic sequence comprises various types of regional and contact metamorphic rocks. Petrography of the major rock units is presented briefly below.

3.c.1. Granitoids

The granitoids vary from granodiorite to monzogranite and syenogranite. In the Khakou area, igneous rocks with intermediate compositions, such as quartz monzonite, are also visible. Petrography of granitoid rocks is as follows.

Quartz monzonite is more abundant in the Khakou area (south Hamedan). This rock is composed of plagioclase, K-feldspar, quartz, biotite, muscovite and zircon (Fig. 4a). Anhedral-granular texture, myrmekite and perthite are its dominant characteristics.

Granodiorite consists of plagioclase, quartz, K-feldspar, biotite, muscovite, apatite, ilmenite and titanite (Fig. 4b). The granodiorite also has fine-grained enclaves enriched in mica, garnet and spinel. Its dominant texture is subhedral-granular. Myrmekite is also present.

The other type of granitoid is mesocratic monzogranite that is observable in several parts of the Alvand plutonic complex. Its main minerals are quartz, plagioclase, orthoclase and microcline. Biotite, muscovite, tourmaline, titanite and zircon are the typical accessory minerals, and sericite is a secondary replacement that is locally developed in the feldspars. Subhedral granular and graphic and granophyric textures, myrmekite and perthite are the most important characteristics of the monzogranite (Fig. 4c).

The syenogranite is holo-leucocratic and consists of quartz, K-feldspar, plagioclase, biotite, muscovite and zircon. Secondary chlorite partially replaces the rare ferromagnesian phases. Anhedral to subhedral granular are the main textures (Fig. 4d). Perthite and myrmekite are also common in this rock.

3.c.2. Pegmatite and aplitite

The pegmatites and aplites intrude the granitoids that are hosted by cordierite-bearing hornfelsic schists and garnet–staurolite schist.

3.c.2.1. Pegmatite. The pegmatites can be divided into two groups, including SBPs and tourmaline–muscovite-bearing varieties. The SBPs are observed only SE of the Khakou area (south Hamedan); they are leucocratic, light grey and coarse-grained. They contain blue corundum (sapphire) with diameters of a few millimetres to more than 1 cm (Figs. 4e, 5). The sapphire crystals are commonly partially converted to sericite and biotite. K-feldspar (microcline and orthoclase, locally perthitic), sodic plagioclase

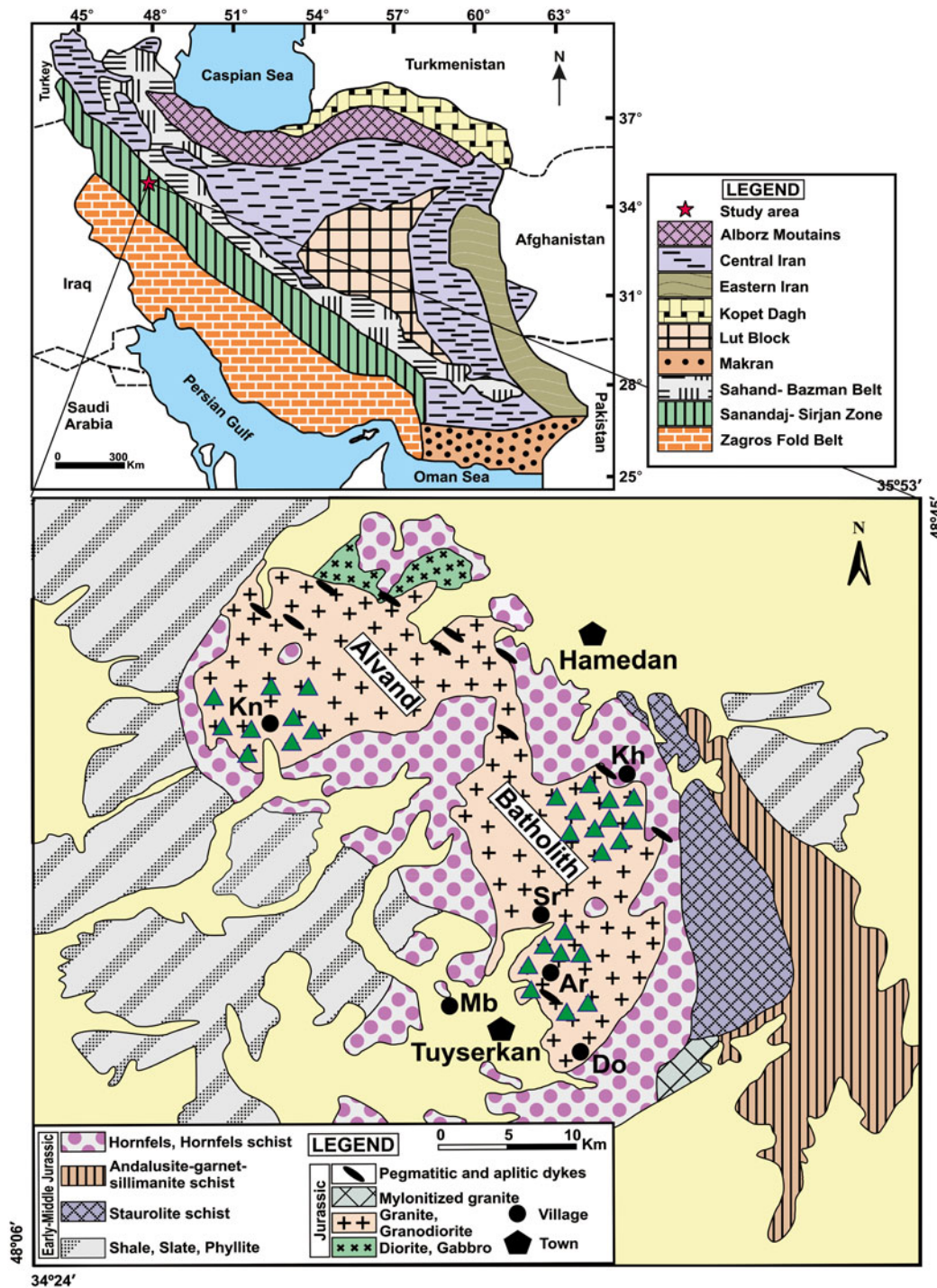


Fig. 2. (Colour online) Lithotectonic map of Iran (modified from Stocklin & Setudenia, 1972) and simplified geological map of the Hamedan region (modified after Sepahi *et al.* 2018). Ar = Artiman, Do = Darreh-Omar, Kh = Khakou, Kn = Kohnoush, Mb = Mobarakabad, Sr = Serkan. Dark green triangles: sampling localities.

and zircon have a dominantly subhedral-granular texture. In some parts of these rocks, tourmaline also occurs. The other group of pegmatites includes leucocratic milky-coloured pegmatites containing large crystals of tourmaline and muscovite, but do not have sapphire. They contain quartz, K-feldspar, plagioclase, muscovite, biotite, tourmaline, garnet, chlorite, zircon and apatite. Subhedral granular and graphic-granophyric textures and perthite are their main textural characteristics.

3.c.2.2. Aplite. The leucocratic and light-grey aplites are less abundant than the pegmatites and occur in some places, such as the Khakou area (south Hamedan). These aplites are composed of

quartz, K-feldspar (microcline and orthoclase), plagioclase, biotite, muscovite, garnet and tourmaline (Fig. 4f) with anhedral granular texture and perthite.

3.c.3. Metamorphic rocks

The metamorphic rocks can be divided into two categories: (1) the contact metamorphic rocks and (2) the regional metamorphic rocks (see also Sepahi *et al.* 2004).

3.c.3.1. Contact metamorphic rocks. These rocks crop out in several parts of the metamorphic aureole of the Alvand plutonic



Fig. 3. (Colour online) (a) The aplites in marginal zone of dykes; (b) alternation of aplite layers with pegmatite layers in a single dyke; (c) tourmaline-bearing pegmatite; (d) sapphire-bearing pegmatites.

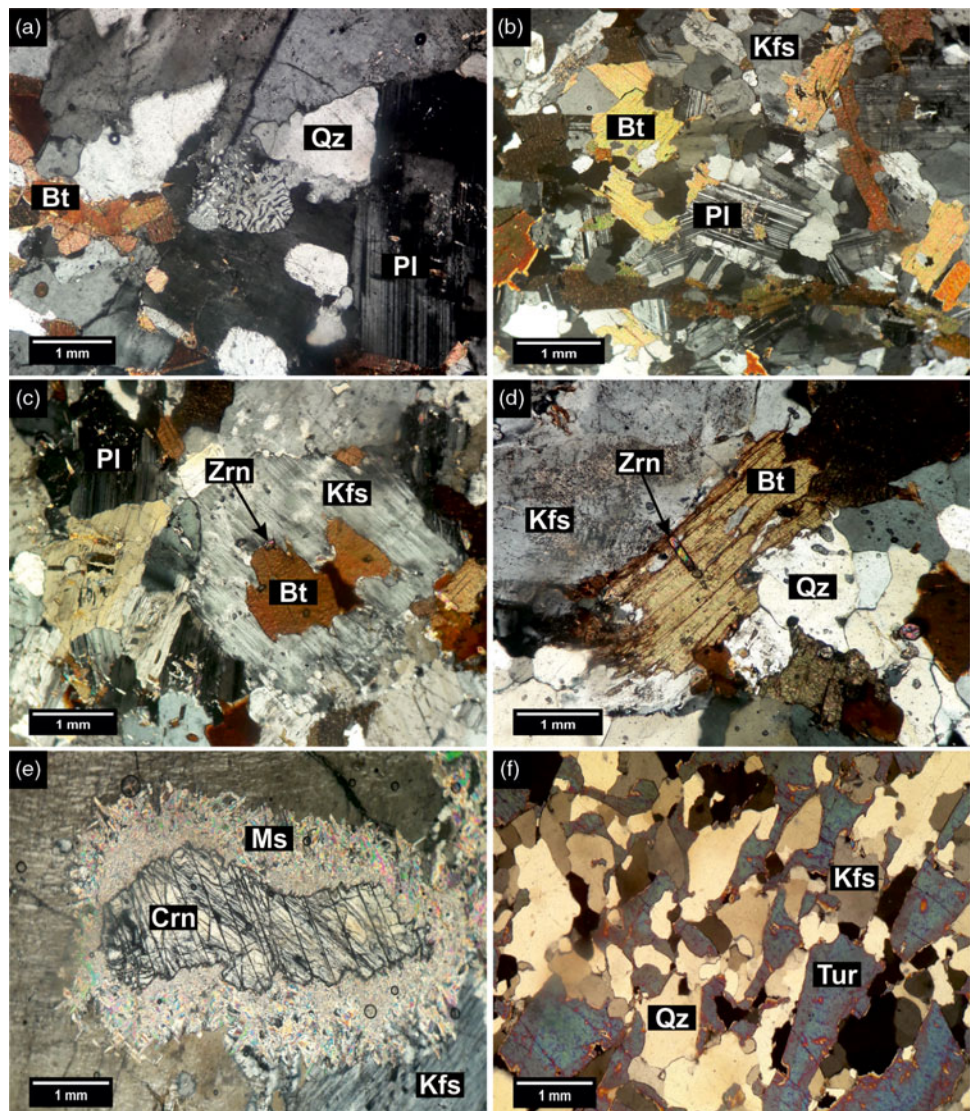


Fig. 4. (Colour online) Photomicrograph of selected granitoid rocks: (a) quartz monzonite, (b) granodiorite, (c) monzogranite, (d) syenogranite, (e) CBP, (f) aplite (mineral name abbreviations according to Whitney & Evans, 2010).



Fig. 5. (Colour online) Close-up of sapphire-bearing pegmatite.

complex. The contact metamorphic rocks include various types of hornfels, such as chlorite–mica hornfels, staurolite–mica hornfels, and cordierite–orthoclase hornfels that were metamorphosed to the albite–epidote and hornblende hornfels facies.

3.c.3.2. Contact metamorphic rocks in the SW Hamedan area. In the Kohnoush area (SW Hamedan), chlorite–mica hornfels occurs as massive, dark grey, fine-grained rock containing biotite as the dominant mineral; it was metamorphosed to the albite–epidote hornfels facies (Supplementary Fig. 1a in Supplementary Material available online at <https://doi.org/10.1017/S0016756820000023>). Its main minerals are granoblastic quartz, biotite, muscovite, plagioclase and chlorite. Sericite and many opaque minerals are secondary.

Granoblastic staurolite–mica hornfels is a massive grey rock with quartz, plagioclase, staurolite and mica (muscovite and biotite) as the main minerals (Supplementary Fig. 1b in Supplementary Material available online at <https://doi.org/10.1017/S0016756820000023>). Sericite (resulting from alteration of biotite) and tourmaline are the secondary phases.

Cordierite–orthoclase hornfels is a dark-grey to black massive rock, containing cordierite, quartz, orthoclase and micas (biotite and muscovite) as the main minerals. Sericite is the only secondary mineral. The biotite locally converts to sericite. This rock shows spotted porphyroblastic texture with cordierite porphyroblasts typical of hornblende–hornfels facies (Supplementary Fig. 1c in Supplementary Material available online at <https://doi.org/10.1017/S0016756820000023>).

3.c.3.3. Contact metamorphic rocks in the south Hamedan and west/northeast Tuyserkan areas. The Khakou area (south Hamedan) hornfels include cordierite hornfels and andalusite hornfels. The cordierite hornfels have porphyroblastic texture due to formation of cordierite and garnet porphyroblasts. Quartz, biotite, muscovite, cordierite and garnet are its main minerals. The andalusite hornfels show migmatitic structures with quartz and feldspathic leucosomes in some parts. Biotite, andalusite, spinel, orthoclase and tourmaline are the most important minerals in them. Porphyroblastic texture is dominant. The other characteristic of these rocks is the occurrence of symplectic andalusite–spinel rim intergrowth (Supplementary Fig. 1d in Supplementary Material available online at <https://doi.org/10.1017/S0016756820000023>). Garnet–staurolite hornfels shows foliation and primary bedding. These rocks have fine-grained staurolite, quartz and biotite.

3.c.3.4. Regional metamorphic rocks. These rocks include slate, phyllite and schist. Slate mostly has a slaty texture, but a spotted texture is observable in some parts. The slates consist of biotite, sericite, quartz, and opaque minerals (iron oxides). Phyllites cropping out in the Kohnoush area (SW Hamedan) are dark-grey to black, and consist of quartz, chlorite, mica and graphite (Supplementary Fig. 1e in Supplementary Material available online at <https://doi.org/10.1017/S0016756820000023>). Garnet–andalusite schist and garnet–staurolite schist occur in many places. The garnet–andalusite schist is composed of garnet, quartz, biotite, andalusite, cordierite and spinel. The garnet–staurolite schist consists of garnet, staurolite, biotite and muscovite (Supplementary Fig. 1f in Supplementary Material available online at <https://doi.org/10.1017/S0016756820000023>).

3.d. Whole-rock geochemistry

In addition to chemical properties of SBPs, the geochemical characteristics of some other pegmatites and associated granitoids of the region are examined and have been compiled from other publications, such as Sepahi (2008), Shahbazi *et al.* (2010), Aliani *et al.* (2012) and Sepahi *et al.* (2018). Whole-rock geochemistry of 28 large samples from the Hamedan area, including 19 granitoid samples, 3 SBP samples (with nearly syenitic composition) and 6 other pegmatite samples (with granitic composition), were determined (Table 1).

The samples are plotted on a TAS (total alkalis vs SiO₂) diagram (Cox *et al.* 1979; Middlemost, 1994) in Figure 6. The granitoids plot in the field of granite and granodiorite on the Cox *et al.* (1979) plutonic rock classification diagram. The SBP samples have different compositions from the other pegmatites and lie near the syenite field (because of their lower SiO₂), whereas the other pegmatites show similarities with granitoids (Fig. 6a). As presented in Table 1, the silica contents of SBPs are significantly lower than those of other pegmatites and granitoids, although their alumina contents are substantially higher. On the TAS diagram (Fig. 6b; Middlemost, 1994), the SBPs are plotted on the foid monzosyenite field and the other pegmatites lie in the granite field. The amounts of molar A/CNK (molar Al₂O₃/(CaO + Na₂O + K₂O)) ratio (Shand, 1943) of the SBPs vary from 2.00 to 2.26, although other pegmatites show lower ratios of 1.01–1.27 (Fig. 7a). Therefore, all pegmatites are peraluminous, but the SBPs are much more peraluminous than the others, which is consistent with their higher contents of Al-rich minerals, such as sapphire and muscovite.

In the I- and S-type granites discriminating plot illustrated in Figure 7b (Chappell & White, 1992), all samples fall in the S-type field. The S-type affinity of these granites and pegmatites of the Alvand plutonic complex has been confirmed earlier by Sepahi (2008), Aliani *et al.* (2012) and Sepahi *et al.* (2018).

Using the Harker diagrams, the SBPs show different geochemical trends from the other pegmatites and the granitoids in both major (Fig. 8) and trace elements (see Supplementary Fig. 3 in Supplementary Material available online at <https://doi.org/10.1017/S0016756820000023>), probably due to their different sources. With increasing SiO₂ as a factor indicating fractional crystallization progress, values of Al₂O₃, Fe₂O_{3t}, CaO and MgO are decreasing and K₂O and Na₂O increase. Zirconium and Hf show descending trends with increasing SiO₂ values (Supplementary Fig. 2 in Supplementary Material available online at <https://doi.org/10.1017/S0016756820000023>), indicating early crystallization of zircon due to decreasing *T*. An increasing trend of Rb against SiO₂ is consistent with late crystallization of K-feldspar and biotite.

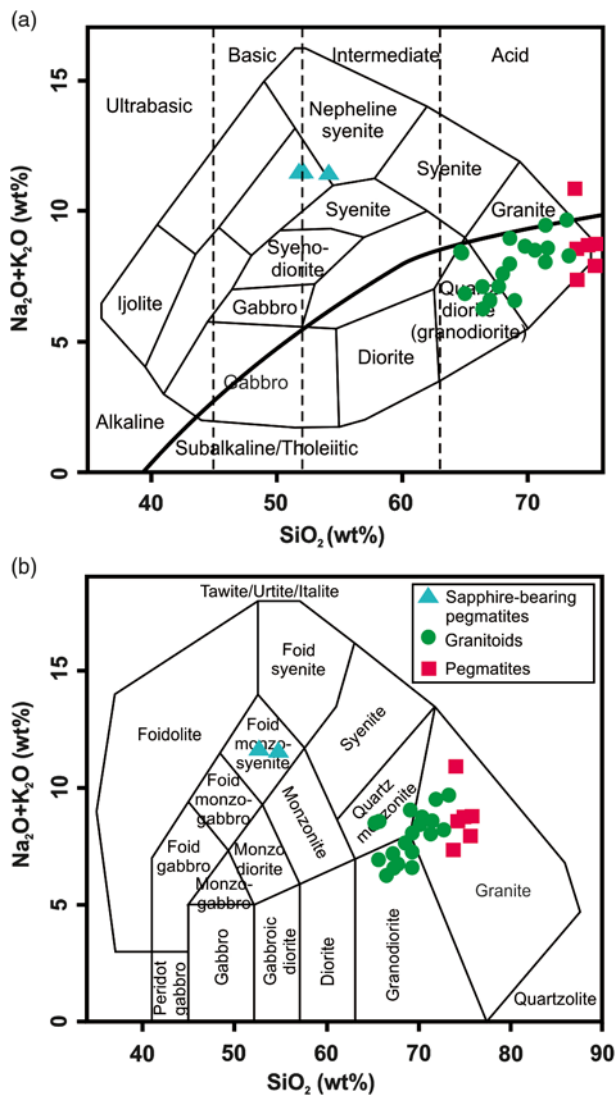


Fig. 6. (Colour online) Plot of chemical composition of the studied samples on chemical classification diagrams. (a) Cox *et al.* (1979), (b) Middlemost (1994).

A descending trend for Sr is compatible with early crystallization of more calcic plagioclase (e.g. Cerný *et al.* 1985; Alfonso *et al.* 2003). Moreover, the following positive correlations are evident due to similar geochemical behaviours of the elements: Ba vs Sr, Rb vs K₂O, Sr vs CaO, and Cs vs Rb (Supplementary Fig. 3 in Supplementary Material available online at <https://doi.org/10.1017/S0016756820000023>).

The chondrite-normalized REE spider diagram shows enrichment of light rare earth elements (LREE) against heavy rare earth elements (HREE) in all samples (Supplementary Fig. 4a in Supplementary Material available online at <https://doi.org/10.1017/S0016756820000023>). This relative enrichment in LREE values and depletion in HREE values (LREE/HREE ratio) is more evident for SBPs than in other pegmatites and granitoids. A negative Eu anomaly in granitoids is more pronounced than in the pegmatites. As a result of the sodic composition of plagioclase and lack of calcic plagioclase and thus deficiency of CaO and Sr values, in which Eu commonly substitutes, most samples exhibit a Eu anomaly. Eu/Eu* in granitoids is in the range 0.19–1.87, in CPBs 0.84–1.90 and in other pegmatites 0.38–6.27 (Table 1). The upper limit of the Eu/Eu* ratio for CPBs is notably lower than

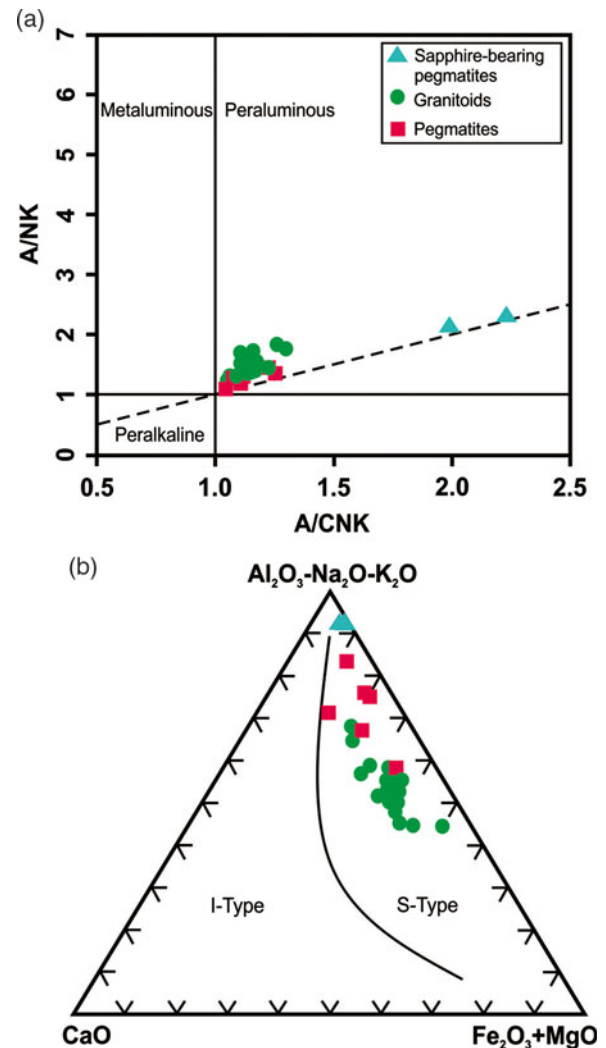


Fig. 7. (Colour online) Plot of chemical composition of the studied samples in (a) Shand (1943), (b) Chappell & White (1992) diagrams.

the upper limit in other pegmatites. The multi-element spider diagram shows negative anomalies for Ba, Nb, Sr, P and Ti that can be attributed to arc-related calc-alkaline magmas that produced the studied samples (Supplementary Fig. 4b in Supplementary Material available online at <https://doi.org/10.1017/S0016756820000023>). Niobium concentrates in refractory parts of the source rocks during melting in subduction zones and leads to a negative anomaly. The negative anomaly of Ti is typically attributed to fractional crystallization of titanite, ilmenite and other Ti-bearing minerals, such as magnetite and biotite and probably muscovite. Positive anomalies of Rb and K that have similar geochemical behaviour are probably due to their relative incompatibility rather than the late crystallization of muscovite and K-feldspar. Negative anomalies of Sr and Ba (with similar geochemical behaviour) can be caused by their concentration in plagioclase in early stages of crystallization. Crystallization of apatite during early-stage crystallization of magma leads to negative anomaly of P in the fractionated rock samples.

The Zr/Hf and Nb/Ta ratios of the studied granitoids and pegmatites (for granitoids, average Zr/Hf = 36.84 and average Nb/Ta = 13.53; for SBPs, average Zr/Hf = 30.41 and average Nb/Ta = 15.54; for other pegmatites, the average Zr/Hf = 27.76 and average Nb/Ta = 5.62) are similar to those ratios for continental crust, and this is in accordance with the S-type

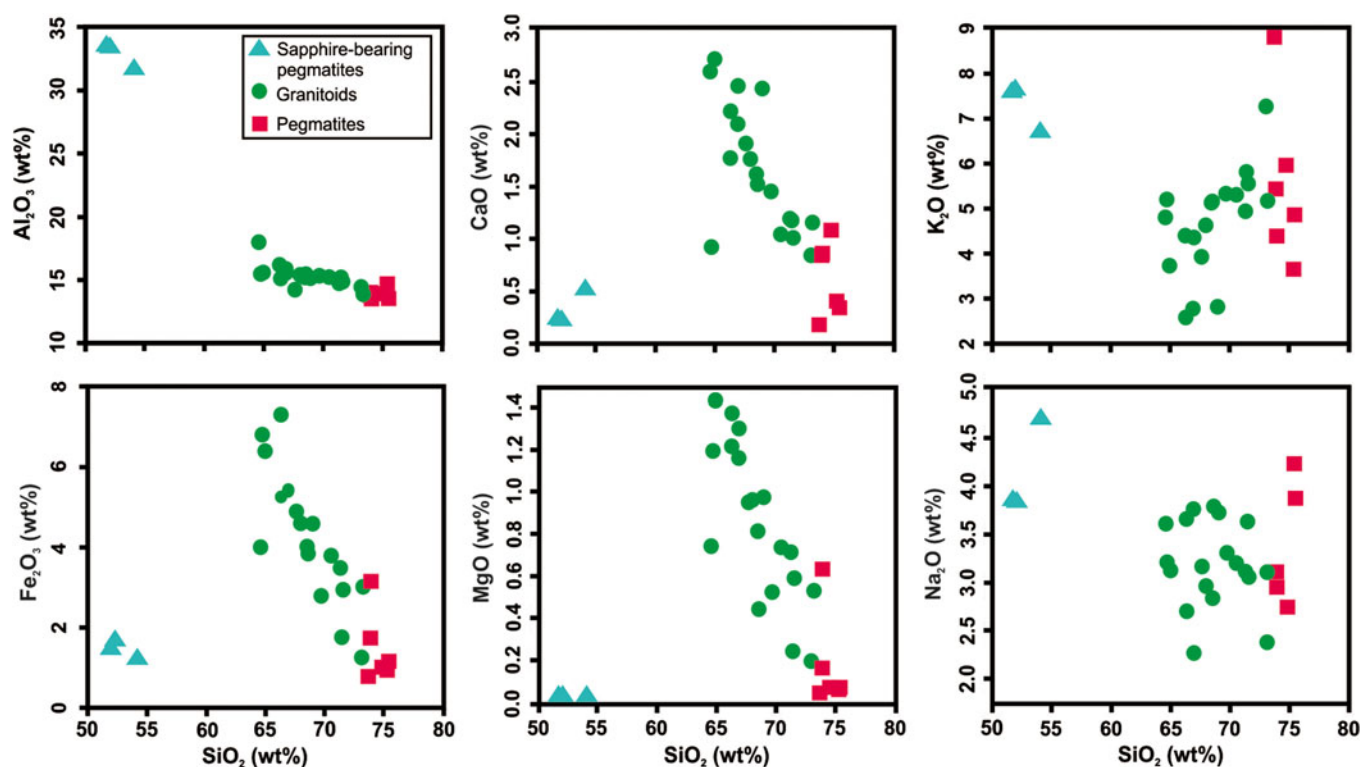


Fig. 8. (Colour online) Harker diagrams of major oxides vs SiO₂ for the studied samples.

affinity of these rocks (Fig. 9; for data references see fig. 8 in Yang *et al.* 2008).

3.e. Discrimination of tectonic setting

Frequently used tectonic discrimination diagrams are presented for the samples: (1) Maniar & Piccoli (1989) and (2) Pearce *et al.* (1984). In the Maniar & Piccoli (1989) diagrams (Supplementary Fig. 5a, b in Supplementary Material available online at <https://doi.org/10.1017/S0016756820000023>), most samples tend to plot in the field of orogenic granitoids (IAG = Island Arc Granitoids + CAG = Continental Arc Granitoids + CCG = Continental Collision Granitoids), although a few samples plot in the anorogenic field (RRG = Rift-Related Granitoids + CEUG = Continental Epirogenic Uplift Granitoids). In the Pearce *et al.* (1984) diagrams (Supplementary Fig. 6a, b in Supplementary Material available online at <https://doi.org/10.1017/S0016756820000023>), most samples tend to plot in the orogenic fields (VAG = Volcanic Arc Granites + Syn-COLG = Syn-Collision Granites (or S-type)) (Christiansen & Keith 1996), but a few samples are in the anorogenic field (WPG = Within Plate Granites). On the basis of results obtained from tectonic discrimination diagrams, a convergent tectonic regime can be considered to occur at the time of magmatic activity in the region. Such a tectonic environment can be commonly inferred for the LCT pegmatites and associated granitoids (Hanson, 2016).

3.f. Geochronology

Because of the existence of geochronological data for plutonic rocks and other pegmatites (e.g. Shahbazi *et al.* 2010; Sepahi *et al.* 2018), only SBPs are selected for zircon geochronology in this study. After petrographic studies and μ XRF mapping, the suitable zircon grains in SBPs were chosen for geochronological and zircon trace-element geochemical studies. μ XRF maps of the zircon grains

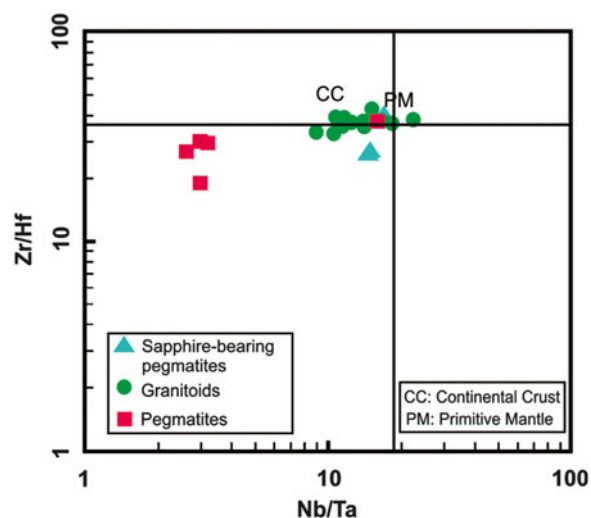


Fig. 9. (Colour online) Plot of Zr/Hf vs Nb/Ta ratios for the studied pegmatites and granitoids.

(Fig. 10) show that some grains are zoned euhedral and others are anhedral. On the Concordia diagram for the SMV-1 sample (Fig. 11a), the weighted mean age is 168 ± 1 Ma with mean square weighted deviation (MSWD) = 0.0115 and a concordance probability of 0.91. The Th/U ratios in its zircons are 0.12–2.44. For the SMV-131 sample, the Concordia diagram (Fig. 11b) shows that the weighted mean age is 166 ± 1 Ma with MSWD = 10.0 and concordance probability of 0.002. The Th/U ratios for the zircons in this sample are 0.05–2.27. The weighted mean age on the Concordia diagram is 164 ± 1 Ma for the SMV-131b sample (Fig. 11c) with MSWD = 1.4 and concordance probability of 0.24. Its zircon Th/U ratios change from 0.09 to 1.54. Combined Concordia for

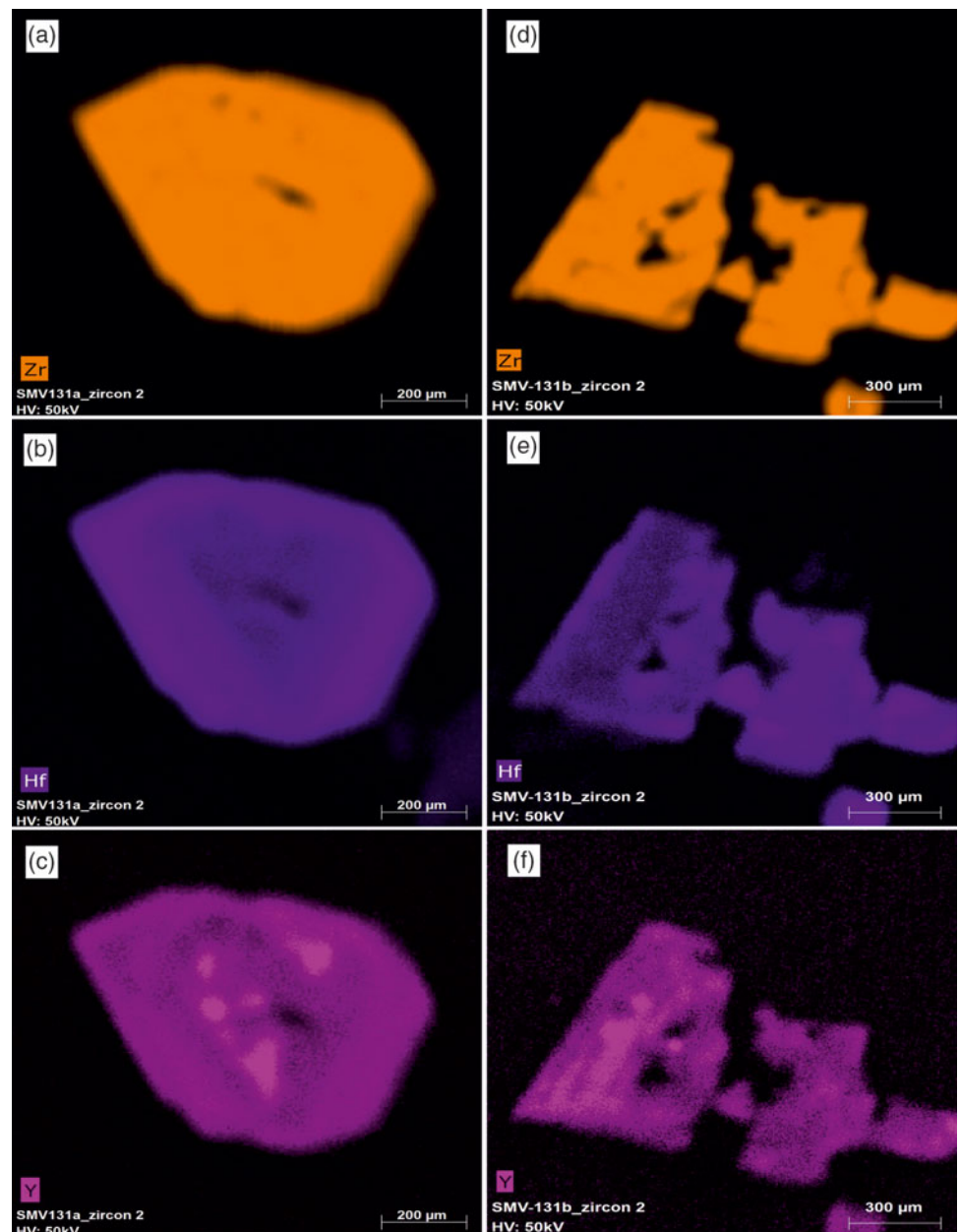


Fig. 10. (Colour online) Micro-XRF maps from zircon grains of sapphire-bearing pegmatites.

samples SMV-131 and SMV131-b is shown in Figure 11d, which indicates a weighted mean age of 165 ± 1 Ma with MSWD = 9.0 and concordance probability of 0.003.

3.g. Zircon geochemistry and thermometry

Zircon is an accessory mineral found in diverse lithologies, such as felsic igneous rocks (e.g. Gao *et al.* 2016), and is host to a variety of trace elements. In addition to Zr, Si and O, minor amounts of Hf and Y and trace amounts of more than 30 elements are reported in zircon (see Table 3). Compositionally, zircon contains *c.* 67.2 wt % ZrO_2 and 32.8 wt % SiO_2 with an additional 0.7–8.3 wt % HfO_2 (with an average of ~ 2 wt %) and Y between 0.1 and 1.0 wt %. Hafnium concentrations in zircon can be elevated in evolved rocks due to magmatic differentiation. REE, Th and U are other important elements taking part in the composition of zircon. In most places, unaltered zircon grains have less than 1 wt % $\Sigma REE + Y$ (e.g. Hoskin & Schaltegger, 2003; Harley & Kelly, 2007; Breiter *et al.* 2016).

The contents of significant trace elements of the zircon grains of SBPs are as follows: Hf values are 3585–17 200 ppm; U from as low as 105 to as high as 13 580 ppm; Th from *c.* 29 to 5148 ppm; Ta from as low as 0.24 to 25.59 ppm; Nb is very variable from 1.46 to 2820 ppm; Y is high in the range 345–4764 ppm, Sc has a narrow range of 244.6–376.6 ppm, Ti also has a narrow range of 5.2–26.2 ppm, and P values change from as low as 1 to as high as 518 ppm. Iron values vary from as low as 9 to as high as 2390 ppm, Al contents are quite variable from 1 to 6360 ppm, Na amounts range from 1 to 4640 ppm, and B contents are between 7 and 124 ppm. ΣREE is in the range 267–2534 ppm, including $\Sigma LREE$ from 3 to 1522 ppm and $\Sigma HREE$ from 189 to 2325 ppm. The amounts of other measured elements, such as Sn, W, Mn, Cr, V, Mg, Li and Be, are quite low (Table 3).

Relative to chondrite values, zircons are strongly HREE-enriched and LREE-depleted, so that in chondrite-normalized spider diagrams there is significant enrichment in HREE against LREE. The trivalent LREE are generally incompatible in the zircon

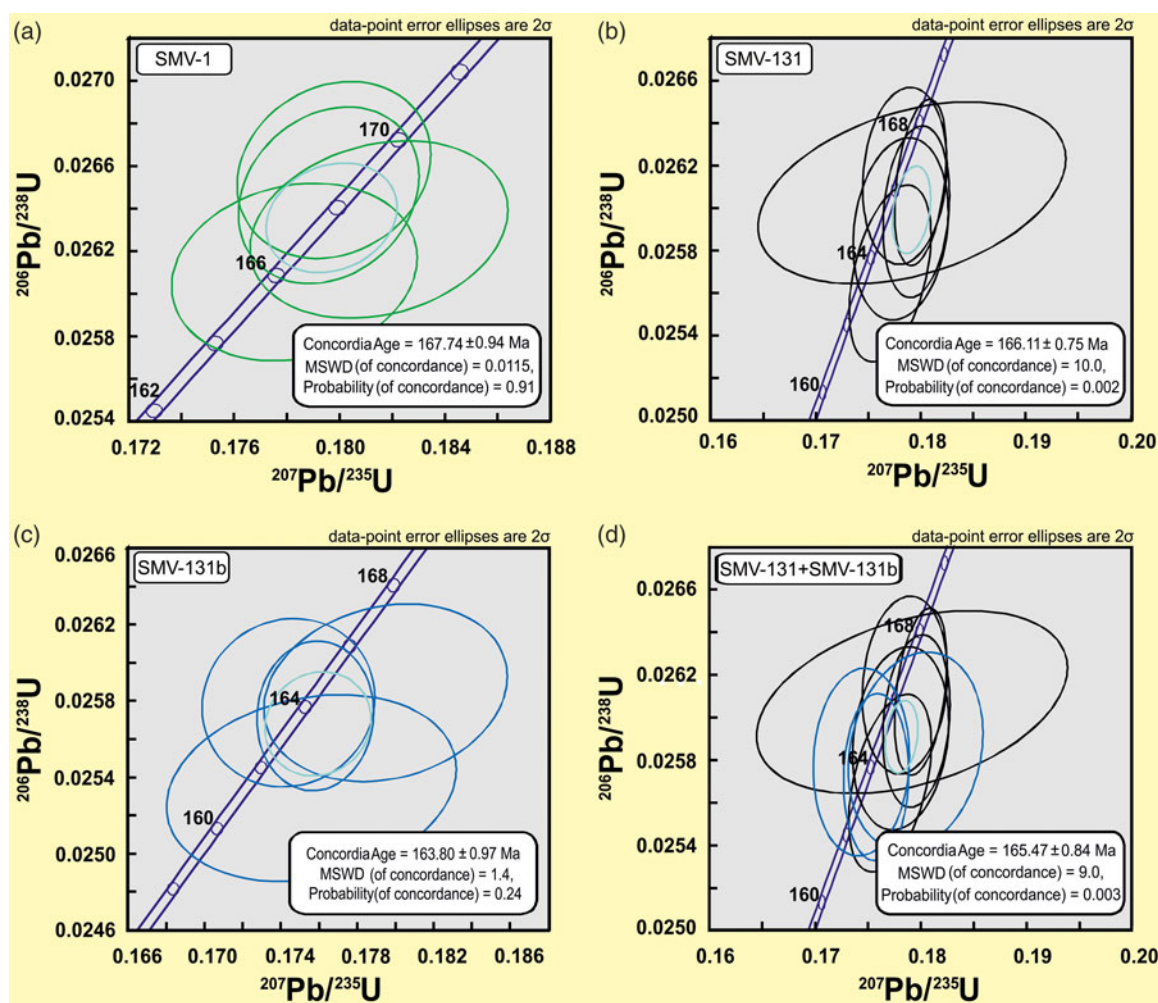


Fig. 11. (Colour online) Concordia diagrams showing calculated U-Pb ages for sapphire-bearing pegmatite samples.

structure so that the absolute abundances of the LREE in igneous zircon are sub-ppm to ppm level. However, this is not the case for Ce, which can be both trivalent and tetravalent, and Ce^{4+} acts compatibly like HREE, so it is abundant in zircon (e.g. Hoskin & Schaltegger, 2003; Trail *et al.* 2012; Nardi *et al.* 2013). Among the REE, Ce and Eu have multiple valence states in magmatic environments, so they can partition differently into zircon structure depending on magma oxidation state (e.g. Ballard *et al.* 2002; Trail *et al.* 2012; Shen *et al.* 2015). On the basis of the Excel spreadsheet by Smythe & Brenan (2016), $\log fO_2 \sim -15$ and $\Delta FMQ \sim -0.3$ estimated for zircons from SBPs. These values mean that a relatively oxidizing environment existed when zircon crystallized from the melt. In the chondrite-normalized spider diagram of the zircons, a positive Ce anomaly is evident (Fig. 12; $Ce/Ce^* = 1.15-68.06$). This reflects the oxidized condition of magma from which the zircon grains crystallized. The divalent Eu cannot easily be substituted for tetravalent Zr, so there is typically a negative Eu anomaly in chondrite-normalized spider diagrams of zircon grains (Fig. 11; $Eu/Eu^* = 0.001-0.56$). These REE features are typical of zircons of magmatic origin.

There is no visible negative or positive correlation between Hf and Y values in the zircons (Fig. 13a). Niobium and Ta values show positive correlation (Fig. 13b). Also, U and Th have positive correlation (Fig. 13c). There is a good positive correlation between

Y and HREE (Fig. 13d). Hafnium and U also show a positive correlation (Fig. 13e). The diagram of P against REE + Y shows no visible correlation (Fig. 13f).

The geochemical characteristics of zircon grains reveal a magmatic origin for zircons of SBPs (Fig. 14a; $(Sm/La)_N$ vs La diagram). The values of La, $(Sm/La)_N$ and Th/U ratios are consistent with a magmatic origin of these zircons (average La < 1.5, $(Sm/La)_N > 100$ and Th/U > 0.7). Also, the studied zircon grains have chemical affinity similar to continental crust zircons (Fig. 14b; U/Yb vs Hf and U/Yb vs Y diagrams; see also Grimes *et al.* 2007).

The correlations between rock type and the trace element compositions of zircon from a wide range of igneous rocks can be shown with a series of discriminant plots. The fields for zircons of some rock types are very distinct, but those for grains of other origins overlap to different degrees in most plots. A single plot is sufficient for the discrimination of zircons from some rocks, but comparison of several plots can identify zircons from some other igneous rocks (see fig. 6 in Belousova *et al.* 2002). In Figure 15, the compositions of the studied zircons are compared with the field of zircons of granitoids from other locations worldwide. Y-U, Y-(Yb/Sm), Y-(Ce/Ce*), (Ce/Ce*)-(Eu/Eu*), Y/(Nb-Ta) and Nb-Ta diagrams are useful for comparing the composition of the studied zircons with zircons in other granitoids (Fig. 15). In these diagrams, chemical compositions of some zircon grains plot

Table 3. Trace element concentrations of zircon grains and calculated Ti-in-zircon crystallization temperatures

Elements (ppm)	SMV-1-1	SMV-1-2	SMV-1-4	SMV-1-5	SMV-1-6	SMV-1-7	SMV-1-8	SMV-1-9	SMV-1-10	SMV-1-12	SMV-1-14	SMV-1-15	SMV-1-16	SMV-1-17	SMV-1-18
Li	1.2	1.4	2.5	2.1	7.6	12.6	3.5	2.5	3.3	1.5	2.4	6.1	1.2	7.2	1.0
Be	7.6	4.1	6.6	3.9	2.7	3.0	5.4	5.0	7.7	6.3	1.1	1.2	3.2	0.6	3.0
B	15.6	16.2	18.1	19.3	14.2	50.7	86.0	16.3	33.5	38.4	15.1	13.8	30.7	20.0	14.6
Na	20.0	11.4	26.0	19.5	3.9	117.7	326.0	10.6	39.0	160.0	64.6	25.9	48.0	417.0	13.5
Mg	2.6	1.6	3.8	2.3	1.2	44.9	5.4	1.0	2.6	7.9	33.0	5.0	4.5	29.3	2.1
Al	18.4	4.5	74.0	11.8	6.9	3570.0	1080.0	9.1	86.0	223.0	474.0	192.0	134.0	151.0	10.1
P	nd	18	29	20	7	134	53	21	nd	56	10	41	40	29	21
Ca	9	21	68	75	38	101	70	30	50	80	155	21	75	234	28
Sc	348.2	322.2	307.0	311.7	314.6	316.0	302.3	308.0	301.5	324.0	299.3	298.7	302.6	294.4	302.0
Ti	13.0	12.8	17.4	14.9	13.7	21.3	26.2	14.3	16.0	15.2	12.2	12.3	14.5	9.8	13.0
V	0.2	0.1	0.1	0.1	0.1	1.2	0.2	0.1	0.2	0.7	0.4	0.2	0.1	0.5	0.1
Cr	2.1	2.6	3.2	3.1	2.9	3.5	2.7	2.2	1.9	3.2	3.1	3.1	3.5	3.5	2.4
Mn	4.5	1.9	5.1	5.1	4.7	132.0	33.0	4.3	13.9	13.7	4.2	3.4	19.9	1.7	5.0
Fe	56.1	26.2	122.6	98.4	155.6	1990.0	560.0	112.1	169.0	550.0	1310.0	210.0	166.0	236.0	53.5
Y	4516	3401	2587	1416	1631	1372	3240	2330	3310	4450	1970	731	1904	482	2256
Nb	6.0	3.9	18.6	23.8	35.1	96.2	42.2	19.3	39.2	14.2	6.3	75.0	8.9	28.5	8.5
Sn	0.8	0.6	2.7	1.4	5.7	1.9	2.3	3.3	4.0	1.1	0.7	0.6	1.1	0.7	0.4
La	0.1	0.3	1.9	1.0	2.6	0.8	1.2	1.1	4.4	0.4	0.1	0.2	0.5	0.2	0.1
Ce	44.1	33.9	244.0	136.8	416.1	13.1	88.1	254.0	340.0	33.6	15.8	2.8	34.2	6.9	23.2
Pr	0.7	1.3	10.0	6.4	19.7	1.1	5.1	8.1	16.7	0.7	0.1	0.2	1.5	0.2	0.3
Nd	14.5	18.7	125.5	87.0	256.3	18.6	61.0	107.3	186.0	10.1	2.4	1.5	17.1	2.7	4.4
Sm	38.2	23.5	111.8	76.8	228.5	28.7	57.5	116.2	136.8	18.9	5.9	1.9	13.2	2.6	9.6
Eu	10.3	7.6	30.1	10.7	34.0	0.7	9.0	26.4	39.2	6.1	2.4	0.4	3.8	0.6	4.0
Gd	196.1	94.1	247.0	149.8	399.4	68.2	155.3	274.0	292.0	100.8	38.4	8.5	44.2	7.4	49.1
Tb	53.7	27.9	50.2	27.3	63.3	15.0	38.7	53.2	57.6	31.6	13.6	4.3	12.9	2.2	16.6
Dy	491.0	292.5	349.0	180.3	321.9	123.4	336.5	341.0	418.0	357.0	152.9	51.0	144.3	27.6	181.6
Ho	119.3	87.8	69.4	37.0	43.4	35.9	89.5	61.5	88.1	117.1	49.6	18.4	50.0	10.4	58.2
Er	364.4	309.3	186.7	116.4	88.0	150.3	311.0	153.4	249.5	451.1	201.2	94.6	207.8	51.6	219.3
Tm	63.9	58.3	31.7	23.1	12.7	35.3	58.8	24.5	41.7	87.6	42.9	24.1	44.3	12.7	43.0
Yb	503.0	477.0	233.5	196.3	83.1	328.0	477.0	176.0	315.3	730.0	397.0	262.0	398.3	130.6	365.0
Lu	68.6	67.1	29.6	30.9	8.4	57.4	70.7	20.1	40.5	110.9	68.5	51.2	67.6	22.1	56.7
Hf	5181	4342	4950	4920	6097	6470	5197	5362	4447	4120	4288	4472	4075	4824	5431
Ta	0.7	0.5	3.1	3.2	2.5	14.3	5.3	1.5	3.4	1.8	0.7	13.6	1.7	2.5	5.6
W	0.1	0.1	0.1	0.1	0.1	4.1	4.1	0.1	0.5	0.6	0.2	6.1	0.6	0.1	0.1
Th	308	222	3190	1552	4001	2530	3900	3080	4890	295	88	133	527	154	200
U	783	443	1670	1492	2619	2080	2260	1838	2075	615	285	782	823	1141	422
∑REE	1967	1499	1720	1079	1977	876	1759	1616	2225	2055	990	521	1039	277	1031
∑HREE	1663	1320	950	611	620.90	745	1382	829	1210	1885	925	505	925	257	940
∑LREE	303	179	770	468	1356	131	377	787	1015	170	65	15	114	20	90
Eu/Eu*	0.27	0.40	0.50	0.27	0.31	0.04	0.25	0.40	0.546	0.32	0.34	0.25	0.41	0.34	0.43
Ce/Ce*	17.40	6.72	6.69	5.94	5.88	2.64	4.64	8.69	5.429	11.38	25.70	3.72	5.85	6.27	24.37
Zr/Hf	81.06	93.50	82.02	82.72	66.59	60.27	73.69	75.34	90.84	100.48	95.38	93.02	102.33	85.61	75.67
T (°C)	764	762	791	776	769	811	832	773	783	778	758	759	774	739	764

Table 3. (Continued)

Elements (ppm)	SMV-1-19	SMV-1-121	SMV-1-22	SMV-1-23	SMV-1-24	SMV-1-25	SMV-1-26	SMV-1-28	SMV-1-30	SMV-131-1	SMV-131-2	SMV-131-3	SMV-131-4	SMV-131-5	SMV-131-6
Li	1.7	0.5	0.7	1.6	11.3	3.1	6.0	10.6	2.5	1.0	10.6	2.2	24.1	0.2	1.3
Be	1.6	0.4	2.1	2.0	1.3	0.5	3.2	4.0	1.6	1.5	0.6	3.3	1.0	0.9	1.9
B	17.1	13.1	11.5	34.7	14.4	10.6	124.4	85.1	32.4	18.0	16.1	32.9	9.0	7.0	17.7
Na	84.0	8.9	12.9	77.0	11.0	32.4	548.0	417.0	4640.0	27.9	64.0	87.7	31.0	18.5	5.0
Mg	8.1	1.8	1.6	3.9	4.0	2.6	7.6	69.0	15.3	74.0	11.3	13.4	7.3	2.4	0.7
Al	151.0	3.8	15.9	200.0	106.9	1.2	2260.0	2130.0	6360.0	2200.0	160.0	2710.0	172.0	1.7	5.7
P	247	14	43	30	39	26	518	167	nd	46	60	18	35	14	5
Ca	143	34	48	37	48	38	117	203	444	137	79	87	44	47	29
Sc	294.2	299.7	302.0	302.7	290.6	307.9	353.3	376.6	257.8	277.1	286.1	289.5	284.6	291.9	298.2
Ti	15.70	9.3	9.7	16.0	13.3	8.1	nd	nd	14.2	16.7	16.5	11.6	7.3	5.2	11.2
V	21.1	0.1	0.1	0.1	0.4	0.1	6.4	3.6	0.2	1.2	1.2	0.2	0.2	nd	0.1
Cr	2.6	3.4	2.7	3.6	2.0	2.5	2.8	3.0	3.1	2.3	2.6	3.5	2.4	3.7	3.7
Mn	5.6	0.8	1.3	29.4	3.5	1.1	39.6	121.0	225.0	14.0	3.6	18.6	1.7	1.7	5.5
Fe	650.0	13.0	84.0	161.0	123.4	19.4	1110.0	2390.0	540.0	1770.0	1017.0	210.0	184.0	12.2	19.4
Y	823	777	1854	1284	388	291	2425	3361	955	3787	860	4764	375	2551	4510
Nb	72.0	1.5	7.6	16.3	19.5	6.9	640.0	2820.0	5.7	16.8	47.6	4.9	11.1	4.3	4.0
Sn	0.6	0.2	1.0	0.4	0.6	0.2	4.1	2.1	1.2	3.2	15.3	4.4	0.4	0.6	0.7
La	13.8	nd	1.8	0.1	0.2	0.1	16.4	3.5	0.5	0.7	7.0	0.1	0.1	0.2	0.1
Ce	46.7	6.0	71.2	8.2	17.2	1.9	293.0	51.9	27.0	38.3	129.0	31.5	0.7	25.2	30.5
Pr	6.6	0.1	5.7	0.1	0.4	0.1	47.8	5.6	0.7	1.1	10.2	0.2	0.1	1.0	0.2
Nd	46.4	1.1	62.1	2.2	5.6	0.8	518.0	85.8	8.7	11.9	100.0	4.2	0.3	13.3	4.4
Sm	22.8	2.8	48.9	5.6	7.5	1.9	312.0	110.3	9.7	14.0	68.4	10.9	1.0	17.8	10.4
Eu	3.9	1.1	15.0	1.7	1.4	0.5	1.7	2.5	3.3	5.0	9.4	4.5	0.1	6.8	4.5
Gd	38.2	14.6	109.1	35.1	21.0	7.7	334.0	203.8	33.6	63.5	119.0	70.9	7.5	69.4	73.4
Tb	8.7	5.1	25.2	10.5	4.3	2.2	53.8	44.6	8.9	20.9	20.5	26.1	2.7	21.1	27.0
Dy	76.6	58.8	203.9	107.3	34.0	21.8	329.0	357.0	84.2	255.9	125.0	328.4	30.9	221.8	324.8
Ho	21.7	19.8	49.6	32.8	9.6	7.3	67.7	94.1	24.5	99.9	23.2	125.2	11.2	70.2	115.9
Er	86.4	81.2	162.0	128.0	48.0	34.8	209.6	334.7	93.5	462.7	72.3	554.0	52.7	276.6	485.0
Tm	20.2	17.0	30.2	27.2	13.8	9.0	36.7	64.9	18.8	98.1	14.0	113.8	12.2	55.7	100.2
Yb	196.9	153.1	243.6	257.9	156.7	97.2	277.7	527.1	165.7	883.0	125.9	1005.0	113.7	481.0	885.0
Lu	33.1	24.5	33.9	45.9	32.0	17.1	37.2	76.6	26.3	155.6	21.4	173.1	20.0	75.2	146.8
Hf	4199	5745	4111	4350	5777	5889	8660	7170	5620	3664	8160	4470	17 190	4140	4097
Ta	6.4	0.2	0.9	2.3	12.4	2.8	70.0	19.9	1.5	1.8	5.1	0.8	4.9	0.4	0.7
W	1.0	0.1	0.1	0.5	0.2	0.1	11.5	126.0	0.9	0.3	0.4	0.2	0.1	0.1	0.1
Th	8100	29	503	129	338	35	21700	2620	301	583	1540	219	179	213	218
U	1730	105	395	454	888	309	6900	2049	310	785	1500	465	1706	372	474
ΣREE	621	385	1062	662	351	202	2534	1962	505	2111	845	2447	253	1335	2208
ΣHREE	443	359	748	609	298	189	1011	1499	421	1976	402	2325	243	1201	2084
ΣLREE	178	25	313	53	53	12	1522	463	83	134	443	122	9	133	123
Eu/Eu*	0.37	0.39	0.56	0.25	0.29	0.31	0.01	0.04	0.47	0.39	0.29	0.34	0.02	0.48	0.34
Ce/Ce*	1.15	29.02	3.27	15.96	10.53	14.44	1.59	2.19	8.71	8.04	2.94	37.95	3.91	7.06	34.25
Zr/Hf	97.16	72.93	100.46	95.86	70.97	71.31	41.57	54.81	63.34	107.80	49.63	91.49	23.85	102.17	103.73
T (°C)	781	734	738	783	766	722	nd	nd	772	787	786	753	714	686	750

Table 3. (Continued)

Elements (ppm)	SMV-131-7	SMV-131-9	SMV-131-10	SMV-131-11	SMV-131-12	SMV-131-13	SMV-131-15	SMV-131-16	SMV-131-17	SMV-131-18	SMV-131-19	SMV-131-20	SMV-131-21	SMV-131-22	SMV-131-23
Li	4.4	0.8	2.1	2.4	0.2	6.2	0.8	nd	0.3	34.8	1.3	1.9	6.6	1.0	6.3
Be	0.4	2.2	1.2	3.4	2.9	1.2	1.4	1.5	1.5	3.0	0.7	0.7	0.6	1.0	0.4
B	15.4	20.1	14.1	13.0	13.3	12.3	6.9	9.7	8.1	7.7	8.1	20.9	8.0	11.9	10.3
Na	33.1	18.7	66.0	4.1	33.0	11.0	5.3	11.3	7.6	39.3	3.9	12.2	3350.0	1.8	0.6
Mg	16.5	2.9	3.0	2.5	1.8	5.2	0.3	1.4	0.5	62.5	0.5	1.6	4.0	1.2	0.4
Al	470.0	16.3	4.3	23.4	3.2	102.0	2.2	1.5	4.1	1800.0	1.8	23.4	5800.0	5.2	1.0
P	68	25	6	31	24	25	56	14	33	167	26	nd	40	36	110
Ca	79	59	110	100	51	59	48	13	19	141	nd	54	248	nd	25
Sc	276.1	302.5	285.8	285.7	296.3	279.1	283.9	290.0	302.4	278.2	284.9	292.2	244.6	284.9	293.7
Ti	13.9	11.10	5.6	12.9	9.1	9.6	11.5	8.4	10.2	12.3	10.8	11.8	11.6	8.7	8.3
V	1.7	0.1	0.1	0.1	0.1	0.1	0.1	0.1	0.1	2.2	0.1	0.1	0.3	0.1	0.1
Cr	2.0	2.4	3.0	3.5	2.9	2.9	2.5	2.9	3.0	1.9	3.4	3.7	2.9	3.3	2.5
Mn	4.4	4.4	0.6	1.2	1.8	4.4	0.6	1.2	1.6	12.0	1.1	1.8	4.7	2.4	1.3
Fe	456.0	24.2	22.3	62.4	16.9	226.0	15.6	15.1	24.5	2020.0	38.0	9.3	2170.0	28.9	47.6
Y	712	4235	2362	4250	4190	1590	2198	3530	3428	2754	830	3465	361	2620	708
Nb	53.0	4.5	8.3	25.7	3.7	25.0	29.2	2.86	2.5	128.9	4.1	6.7	17.3	4.3	37.9
Sn	1.3	0.8	1.5	2.5	0.5	0.7	1.1	0.4	0.4	3.1	0.2	1.8	2.2	0.9	0.2
La	19	0.1	0.1	0.4	0.1	0.2	0.1	0.1	0.1	1.4	nd	0.1	1.5	1.3	0.1
Ce	20.6	30.4	59.2	162.8	24.7	1.6	0.6	19.1	16.5	6.6	3.5	19.8	6.7	42.3	0.3
Pr	3.3	0.2	0.6	3.4	0.2	0.1	0.1	0.1	0.3	0.8	0.1	0.1	0.5	3.4	0.1
Nd	17.3	4.9	11.3	48.1	5.5	0.7	0.5	1.9	6.9	6.7	0.3	2.4	6.4	36.5	0.1
Sm	8.9	13.0	19.3	55.6	15.2	3.5	4.2	5.6	21.1	19.1	1.1	5.6	9.2	34.0	0.1
Eu	2.3	4.9	5.6	17.6	3.7	0.1	nd	2.8	3.0	0.4	0.5	2.8	0.2	10.8	0.1
Gd	19.0	86.4	85.1	181.4	90.6	27.8	34.8	43.7	121.4	100.3	8.9	45.0	24.7	96.0	2.1
Tb	4.9	29.7	23.7	45.2	30.0	11.4	14.6	17.1	35.1	31.4	3.7	17.4	5.3	25.6	1.4
Dy	50.6	328.0	224.9	408.1	321.2	134.0	171.8	225.4	328.0	291.8	51.0	224.9	39.2	238.6	32.0
Ho	18.8	107.5	62.0	116.3	110.9	46.9	64.4	90.8	86.8	84.6	22.3	89.8	10.3	72.8	18.5
Er	98.9	429.2	217.4	415.3	488.0	216.0	309.2	429.7	293.1	328.5	112.0	413.1	43.1	284.8	107.4
Tm	25.6	86.7	40.8	75.1	101.0	47.9	72.2	95.1	53.3	64.8	26.3	89.0	9.7	56.3	27.4
Yb	278.3	752.0	327.0	590.0	890.0	434.0	663.6	868.0	429.0	530.5	257.0	791.0	95.0	479.5	282.8
Lu	59.0	119.2	46.6	86.8	153.0	72.2	112.2	158.0	61.0	79.9	50.1	139.4	15.6	76.6	52.1
Hf	3895	4426	5218	4094	4455	15 590	15 910	3660	5776	14 800	4544	3840	11 370	3585	5619
Ta	4.1	0.6	0.9	1.9	0.6	7.2	11.1	0.4	0.4	25.6	1.3	0.6	1.6	0.3	17.2
W	0.3	0.1	0.1	0.1	0.1	0.1	0.1	0.1	0.1	6.1	0.1	0.3	3.9	0.1	0.1
Th	490	165	995	2907	203	248	250	142	162	5148	117	167	390	301	152
U	948	426	997	1605	577	2480	3318	370	601	13580	457	484	922	329	1167
ΣREE	626	1992	1123	2206	2234	996	1448	1957	1455	1546	536	1840	267	1458	524
ΣHREE	536	1852	942	1736	2094	962	1408	1884	1286	1411	522	1764	218	1234	521
ΣLREE	90	139	181	469	139	34	40	73	169	135	14	75	49	224	3
Eu/Eu*	0.48	0.31	0.33	0.45	0.22	0.01	0.01	0.35	0.13	0.02	0.33	0.35	0.03	0.50	0.03
Ce/Ce*	0.57	38.95	26.55	13.33	27.67	3.23	16.07	54.16	15.37	1.49	68.06	48.42	1.76	3.14	14.23
Zr/Hf	104.23	94.89	80.10	101.61	92.92	25.97	25.95	113.93	72.36	26.48	92.86	110.67	31.48	117.99	74.92
T (°C)	770	750	692	763	732	737	753	725	742	759	747	755	753	728	724

Table 3. (Continued)

Elements (ppm)	SMV-131b-1	SMV-131b-2	SMV-131b-3	SMV-131b-4	SMV-131b-5	SMV-131b-6	SMV-131b-7	SMV-131b-8	SMV-131b-9	SMV-131b-10	SMV-131b-11	SMV-131b-12	SMV-131b-13	SMV-131b-14	SMV-131b-15	SMV-131b-16
Li	6.2	0.3	11.5	1.1	2.8	10.5	2.8	0.6	0.4	9.5	9.6	22.7	0.6	1.8	0.5	2.2
Be	0.7	0.1	0.5	3.2	2.7	1.3	0.8	0.4	0.1	0.9	0.9	0.7	0.7	0.1	1.8	4.0
B	14.7	13.3	13.5	15.7	22.6	8.3	24.0	9.1	9.4	20.6	9.9	11.6	12.2	9.6	14.2	25.0
Na	79.1	9.0	12.6	98.1	108.0	8.2	10.0	9.9	5.1	63.9	30.2	52.0	43.9	2.6	3.0	6.6
Mg	40.3	1.4	1.1	4.5	1.4	6.8	1.8	1.3	2.0	1.5	25.5	4.9	5.4	0.7	0.7	1.2
Al	500.0	2.14	8.0	324.0	182.0	460.0	28.5	3.1	2.5	82.0	312.0	4.2	4.2	0.9	2.8	9.1
P	51	21	51	31	29	24	1	17	nd	36	72	35	1	10	20	17
Ca	177	36	82	114	99	36	66	60	109	69	114	92	40	79	nd	14
Sc	276.9	283.6	290.2	289.3	291.8	281.2	279.9	293.1	289.1	281.6	275.0	280.0	282.2	285.3	281.1	281.8
Ti	10.6	8.7	8.40	10.30	9.80	7.20	12.60	9.20	9.90	6.00	9.10	6.20	10.60	8.70	12.80	12.40
V	1.1	0.1	0.1	0.3	0.1	0.1	0.1	0.1	0.1	0.1	0.3	0.1	0.1	0.1	0.1	0.1
Cr	3.2	2.6	3.2	3.6	3.3	3.5	2.2	1.8	2.6	2.5	2.8	2.1	2.4	2.8	1.9	2.1
Mn	7.9	2.0	1.0	4.7	6.1	1.4	3.8	1.6	0.9	2.4	3.1	0.5	1.2	1.1	0.6	5.8
Fe	770.0	29.1	16.5	580.0	59.2	153.0	95.5	31.5	26.5	57.5	401.7	11.8	58.7	37.4	48.3	68.1
Y	346	446	238.20	4364	2930	1406	4522	4108	641	708	1340	405	809	345	3415	4679
Nb	22.7	5.2	11.1	11.3	8.5	21.7	30.9	2.4	2.8	7.1	31.4	9.8	5.2	2.8	12.0	18.2
Sn	2.6	0.2	0.2	1.3	0.5	1.0	3.3	0.6	0.3	0.6	0.9	0.4	0.9	0.2	1.6	2.2
La	1.3	nd	0.1	0.5	0.1	0.1	0.9	0.1	0.1	0.2	0.2	0.1	0.1	nd	0.1	0.4
Ce	32.7	1.4	4.4	22.2	18.9	5.1	210.1	20.2	6.8	24.5	1.3	0.3	41.4	0.1	89.9	152.1
Pr	3.1	0.1	0.2	0.4	0.2	0.1	5.8	0.3	0.6	1.1	0.2	nd	1.2	nd	1.2	3.3
Nd	30.1	0.2	2.3	7.2	4.7	1.4	76.7	6.11	9.4	11.9	1.1	0.1	17.1	0.1	17.4	46.3
Sm	26.2	0.4	1.8	16.7	12.4	6.2	81.0	18.0	15.5	11.30	3.5	1.5	22.9	0.5	27.4	55.0
Eu	1.0	0.1	0.5	4.0	3.9	0.4	22.5	3.8	1.0	2.8	0.1	nd	3.7	nd	9.2	18.0
Gd	36.2	3.0	5.8	100.1	79.0	37.3	231.2	97.1	43.7	29.9	23.5	9.6	67.4	4.9	116.3	190.0
Tb	6.4	1.3	1.6	35.5	26.8	13.0	54.1	30.5	10.7	7.6	9.4	3.4	15.4	2.0	32.6	48.9
Dy	41.1	21.2	17.74	393.7	275.0	131.6	460.5	320.1	81.7	70.8	110.9	37.2	106.7	24.9	312.9	446.5
Ho	9.7	11.3	7.0	110.1	76.4	39.9	123.8	101.8	17.2	20.2	39.4	12.1	20.8	9.8	92.1	128.6
Er	39.6	70.7	36.7	365.9	257.0	165.3	419.5	391.2	50.3	78.6	188.3	54.3	57.3	52.2	332.4	463.3
Tm	9.3	19.0	9.6	65.4	47.8	34.6	74.0	75.0	9.0	16.1	42.9	11.9	9.7	13.4	61.8	84.7
Yb	91.6	200.1	102.6	528.6	398.0	295.1	575.9	629.3	70.4	139.4	396.5	108.4	74.1	134.9	494.0	666.3
Lu	15.9	42.2	22.1	75.8	60.0	47.0	83.4	94.0	9.0	23.1	67.9	18.0	9.7	26.5	73.1	99.1
Hf	7610	4959	6180	4511	8290	14 090	4029	5243	6951	6974	16 190	17 200	6213	9880	4398	3948
Ta	6.4	1.4	9.4	1.6	4.1	5.6	2.5	0.5	0.5	2.2	11.3	4.2	0.5	1.1	1.1	2.2
W	0.8	0.1	0.1	1.2	0.1	0.1	0.1	0.1	nd	0.1	0.1	0.1	nd	0.1	0.1	0.1
Th	827	111	131	217	195	689	3593	179	74	561	376	309	704	44	1710	3171
U	1373	376	704	787	826	3400	1920	681	407	1083	4003	2054	847	482	1227	1753
ΣREE	344	371	212	1726	1260	777	2419	1787	325	437	885	256	447	269	1660	2402
ΣHREE	213	365	197	1575	1141	726	1791	1641	248	355	855	245	293	263	1399	1937
ΣLREE	130	5	15	151	119	50	628	146	77	81	30	11	153	6	261	465
Eu/Eu*	0.08	0.24	0.37	0.21	0.26	0.06	0.43	0.21	0.11	0.41	0.02	nd	0.25	nd	0.39	0.45
Ce/Ce*	2.63	49.50	5.33	10.32	21.53	16.64	10.05	20.25	3.32	5.83	1.44	29.18	9.47	nd	21.85	12.78
Zr/Hf	53.61	85.50	68.12	87.34	50.30	29.80	102.50	78.77	60.71	59.21	24.64	23.48	65.50	42.20	93.45	103.34
T (°C)	745	728	725	743	739	712	761	733	739	698	732	700	745	728	762	759

nd = not detected.

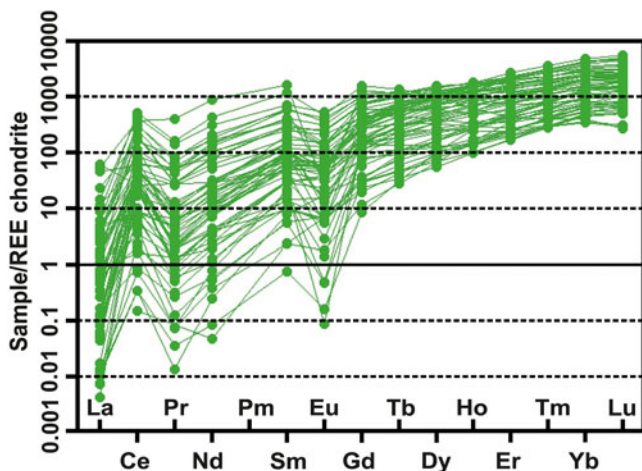
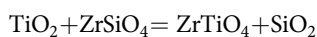


Fig. 12. (Colour online) Chondrite-normalized REE spider diagrams of the studied zircon grains (normalized to Boynton (1984) values).

in the field of previously studied zircon grains of the granitoids and pegmatites of the other places of the world, and of course, some others do not plot in these fields.

Titanium content of zircon has been an important petrogenetic tool in recent years. Therefore, Ti-in-zircon thermometry has been considered in many recent publications in the literature (e.g. Fu *et al.* 2008 and references therein; Hofmann *et al.* 2014). Regardless of some limitations to its usage, it can be applied to estimate crystallization temperatures of igneous zircons. Common limitations for Ti-in-zircon thermometry include variation of TiO_2 or SiO_2 activity, pressure effect, resetting of Ti concentration by subsolidus alteration or diffusion (subsidiary resetting of Ti compositions) and accuracy of the thermometer calibration (errors in calibration).

Watson & Harrison (2005) and Watson *et al.* (2006) experimentally calibrated the titanium concentration in zircon as a function of temperature of formation and the activity of TiO_2 . The theoretical calculations of Harrison *et al.* (2005) and further experiments of Ferry & Watson (2007) suggest the substitution:



In the absence of rutile, Ti can participate in the composition of other minerals in minor and trace amounts. According to Watson *et al.* (2006), the following equations can be used to estimate the temperature of zircon considering its Ti content:

$$\log(Ti_{\text{zircon}}) = [(6.01 \pm 0.03)] - [(5080 \pm 30)/T(K)] \quad (1)$$

$$T^{\circ}\text{C}_{\text{zircon}} = [(5080 \pm 30)/((6.01 \pm 0.03) - \log(Ti))] - 273 \quad (2)$$

On the basis of these equations, temperatures from ~683 to ~828 °C were obtained for crystallization of zircon in SBPs with an average temperature of $755^{\circ} \pm 73$ °C. Details of temperatures calculated for each point of analyses are given in Table 3.

The results of Ti-in-zircon thermometry are compared with zircon and monazite saturation temperatures. Zircon saturation temperatures calculated using the Watson & Harrison (1983) model considering bulk rock Zr concentration as magma composition are calculated (Tables 1, 4). T_{zircon} for granitoids is in the range

644–870 °C with an average of 804 °C, for SBPs it is in the range 614 to 635 °C with an average of 622 °C and for the other pegmatites it is in the range 614 to 832 °C with an average of 688 °C. Monazite saturation temperatures using bulk rock ΣLREE composition (La + Ce + Pr + Nd + Sm + Gd) as melt composition in the Montel (1993) equation are also calculated (Tables 1, 4). T_{monazite} for granitoids ranges from 702 to 869 °C with an average of 810 °C, for SBPs it ranges from 735 to 770 °C, with an average of 748 °C, and for other pegmatites it is between 580 and 843 °C, with an average of 673 °C. Comparison of the results of Ti-in-zircon thermometry with zircon and monazite saturation temperatures indicates that T_{monazite} for CPBs (average = 748 °C) is near the temperature obtained by Ti-in-zircon thermometry (average = 755 °C).

Hafnium contents of zircon grains are 3585–17 200 ppm, and Zr/Hf ratios are 23–117 (Table 3). Therefore, on the basis of the data for granitic and pegmatitic zircons in the database presented in Wang *et al.* (2010), the studied zircon grains have a similar range of Zr/Hf ratios in comparison to other granitic zircons reported in the literature, although they have Zr/Hf ratios in the range which is reported for early crystallized zircons. Histograms of Zr/Hf ratios vs number of zircon grains for SBPs are shown in Supplementary Figure 7 in the Supplementary Material available online at <https://doi.org/10.1017/S0016756820000023>. In contrast to zircons studied by Kirkland *et al.* (2015), our zircons have a similar range of Th/U ratios (0.1–4), but in the case of Zr/Hf ratios some are similar and the others are quite a bit higher (20–120).

4. Discussion

In recent years, the interpretation of various geological aspects, such as geochronology, petrogenesis and tectonic setting of the SSZ of Zagros orogen, has been topical. Examinations of the petrogenesis and geochronology of granitoids and related pegmatites help to decipher some geological enigmas of the region (e.g. Shahbazi *et al.* 2010; Hassanzadeh & Wernicke, 2016; Sepahi *et al.* 2018). In this regard, we have considered an enigmatic type of pegmatite (CPBs) to reveal its possible petrogenetic and geochronological connection with other pegmatites and granitoids of this study area and adjacent areas. In the following three subsections, we use data obtained in this study, together with the results of similar studies on pegmatites and associated granitoids of the region, to provide some helpful data for interpreting the tectono-magmatic history of the SSZ.

4.a. Significance of obtained age data

As noted earlier in Section 2, older data have been obtained by $^{40}\text{K}\text{-}^{39}\text{Ar}$ and $^{87}\text{Rb}\text{-}^{86}\text{Sr}$ methods, giving Late Cretaceous ages for the Alvand plutonic complex (e.g. Valizadeh & Cantagrel, 1975; J Braud, unpub. PhD, Univ. Paris, 1987). Using the same method ($^{40}\text{K}\text{-}^{39}\text{Ar}$), similar Late Cretaceous ages have been obtained (e.g. Baharifar *et al.* 2004), but recent U–Pb geochronological studies have yielded Middle Jurassic ages (e.g. Shahbazi *et al.* 2010; Mahmoudi *et al.* 2011; Chiu *et al.* 2013; see also Section 3.f). Gabbroic rocks formed at 166.5 ± 1.8 Ma, granodiorites–monzogranites between 163.9 ± 0.9 Ma and 161.7 ± 0.6 Ma, and leucocratic granitoids between 154.4 ± 1.3 and 153.3 ± 2.7 Ma (Shahbazi *et al.* 2010). Isotope dilution thermal ionization mass spectrometry (ID-TIMS) U–Pb zircon geochronology by Mahmoudi *et al.* (2011) gave an age of ~165 Ma for phases of the Alvand granite pluton. Also, Chiu *et al.* (2013) have obtained zircon U–Pb ages of 165.1 ± 2.0 and 163.9 ± 1.8 Ma. According to

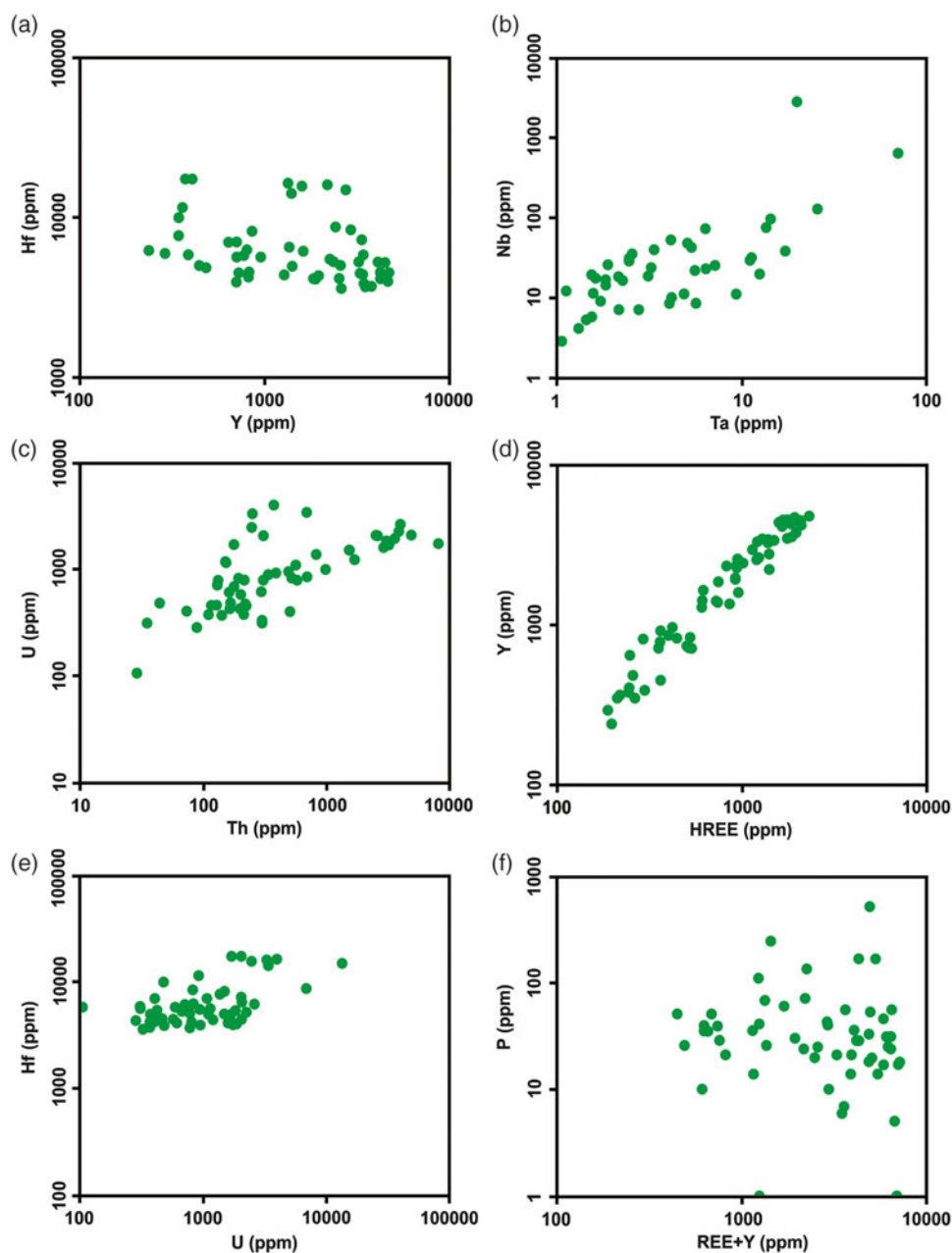


Fig. 13. (Colour online) Distribution of common important trace elements pairs in composition of the studied zircon grains: (a) Hf vs Y; (b) Nb vs Ta; (c) U vs Th; (d) Y vs HREE; (e) Hf vs U; (f) P vs REE + Y.

Sepahi *et al.* (2018), zircon and monazite U–Pb geochronology yielded ages in the range 162–172 Ma for pegmatites and an age as young as 154.1 ± 3.7 Ma for an allanite-bearing pegmatite sample from the Alvand plutonic complex. Also, Yang *et al.* (2018) and Zhang *et al.* (2018a, b) have estimated Jurassic ages for most of these plutonic rocks by zircon U–Pb geochronology. In this study, we have also obtained Jurassic ages for the pegmatites. Also, in neighbouring regions (in the Qorveh–Aligoudarz plutonic belt of the Sanandaj–Sirjan zone (Mohajjel & Fergusson 2014), the main plutonic suites have Middle Jurassic ages (e.g. Ahmadi-Khalaji *et al.* 2007; Esna-Ashari *et al.* 2012). Yajam *et al.* (2015) attributed the age of major plutonic rocks of the Qorveh region in the NW of the Hamedan region to the upper Jurassic. Therefore, we can attribute major plutonic activity and pegmatite generation in this region and adjacent regions in the northwest of SSZ to the Jurassic. The metamorphic events also have an age range of 160–180 Ma (Middle Jurassic) (Sepahi *et al.* 2019), so an overlap

of ages is evident between metamorphism and plutonism in the region. According to Sepahi (2008) and Sepahi *et al.* (2018), plutonism and metamorphism of the region occurred concurrently due to subduction-related tectono-magmatic activities at a continental arc geodynamic regime. Metamorphism slightly predates plutonism, but was intensified by it later (i.e. regionally metamorphosed rocks underwent contact metamorphism later).

4.b. Genetic implications

4.b.1. Geochemical constraints

AA Sepahi (unpub. PhD, Tarbiat Moallem Univ. Tehran, 1999; 2008) and Sepahi *et al.* (2018) have found a genetic link between major pegmatitic dykes and granitoids of the region on the basis of field, petrographic and geochemical characteristics of these rocks. Also, we found that major pegmatitic rocks (mildly peraluminous samples) may have a genetic link with these granitoids, except for

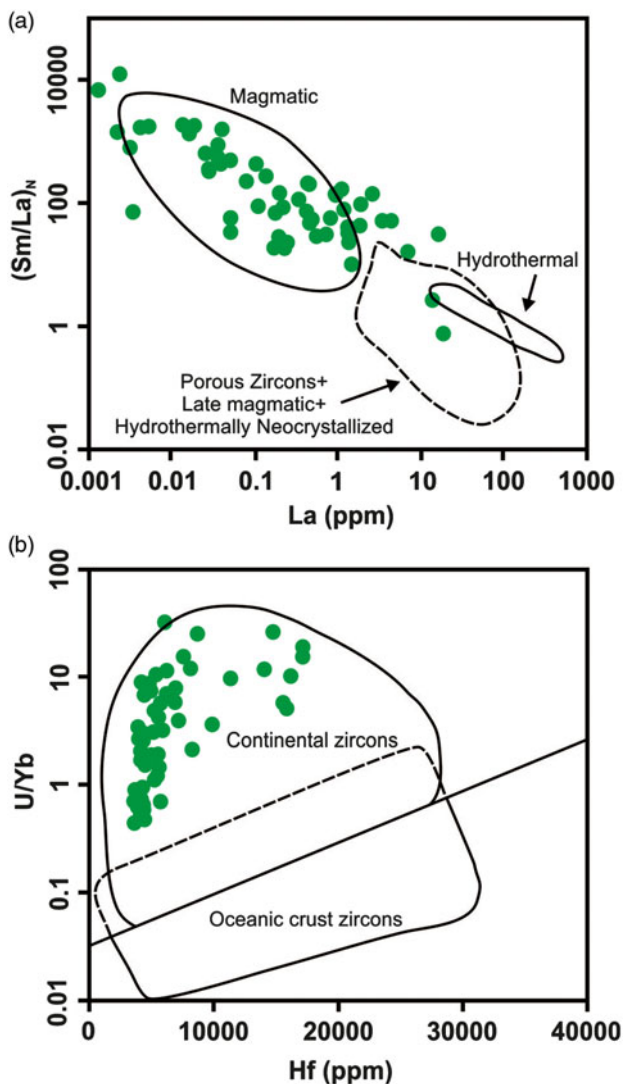


Fig. 14. (Colour online) (a) $(\text{Sm/La})_N$ vs La diagram, which indicates a magmatic origin for zircon grains of SBPs (see also Babazadeh *et al.* 2019 and references therein). (b) U/Yb vs Hf diagram, which reveals that zircons of SBPs have characteristics of continental zircons.

sapphire-bearing syenitoid pegmatites that are the focus of this study. These rocks contain a low content of silica in comparison to other pegmatites and granitoids. They even plot in the field of silica-undersaturated rocks in some diagrams. Also, they are extremely peraluminous ($\text{Al}_2\text{O}_3 > 30$ wt %, $A/\text{CNK} > 2$) and in geochemical and tectonic discrimination diagrams do not show any genetic link with granitoids of the region (see Section 3.d; Fig. 6; Supplementary Figs 3, 4 in Supplementary Material available online at <https://doi.org/10.1017/S0016756820000023>). Therefore, they cannot be fractionated equivalents of these granitoids and other common mildly peraluminous pegmatites of the region. They may be generated from magma originated from partial melting of meta-sedimentary rocks of the region. On the other hand, they have the same age as granitoids of the region and may be formed in the same dynamothermal regime as well.

4.b.2. Possible corundum (sapphire) origin

The various geological aspects of corundum deposits (especially of the sapphire variety) from different countries worldwide (such as Madagascar, Tanzania, Kenya, Malawi, Nigeria, USA, Brazil, Russia,

Afghanistan, Pakistan, India, Sri Lanka, Myanmar, Vietnam, China, Cambodia, Thailand, Australia, France, West Pacific, Colombia, Canada, Greenland, Norway, Greece and Slovakia) have been studied in detail in recent years (e.g. Giuliani *et al.* 2005, 2007, 2009, 2014; Graham *et al.* 2008; Simonet *et al.* 2008; Sutherland *et al.* 2008; Uher *et al.* 2012).

Also, the origin and usage of corundum has been the subject of some recent publications. A lot of classifications have been proposed for corundum deposits by different authors based on various features such as the lithology of the host rocks, the morphology of corundum, the geological context of the deposits, the genetic processes responsible for corundum formation, the type of deposit and the nature of the corundum host rock, and the oxygen isotopic composition of corundum (Giuliani *et al.* 2014 and references therein).

According to Simonet *et al.* (2008), corundum deposits can be classified into two major groups (primary and secondary). Primary deposits are either igneous or metamorphic and secondary ones are either sedimentary (detritic) or igneous (xenocrystic). Primary igneous deposits commonly occur in syenitic rocks. In these rocks corundum is always associated with rocks depleted in silica and enriched in alumina because, in the presence of excess silica, Al is preferentially incorporated into aluminosilicate minerals such as feldspars and micas (Giuliani *et al.* 2014). Metamorphic corundum can be metamorphic (*sensu stricto*), metasomatic and anatectic in origin (Giuliani *et al.* 2014). Thus, many metamorphic rocks (such as skarn, marble, gneiss and migmatite) and igneous rocks (such as kimberlite, alkali basalt, lamprophyre and syenite) may contain corundum.

On the basis of this classification scheme, two possible origins can be assumed for corundum in the studied pegmatite: igneous and metasomatic. As mentioned above, desilication may be a possible process in the petrogenesis of these rocks, but source and evidence for desilication were not observed. There are no signs of metasomatism in nearby sapphire-bearing syenitoid pegmatitic dykes (absence of silica-deficient rocks such as ultramafites and meta-carbonates in accidental and/or tectonic contact with sapphire-bearing dyke); therefore an igneous origin for sapphire in this rare dyke is probable (i.e. country rocks are granitoids and meta-pelitic over-saturated rocks, not ultramafites, foid-bearing under-saturated rocks and/or metacarbonates). On the basis of the geochemical features, it is obvious that sapphire-bearing rocks of the region are not a direct product of differentiation of host granitoids and other pegmatites. According to Giuliani *et al.* (2014), corundum is a typical mineral of pegmatite in syenitic rocks and has been reported in these rocks from Russia, Canada, India and Norway. Simonet *et al.* (2004) studied the Tula corundum deposit hosted by dykes of syenite, in Garba Tula, Kenya. In this deposit corundum is formed by direct crystallization from a magmatic melt as an accessory mineral phase. Corundum of the studied SBPs may have a similar origin. However, it should be noted that gemstone production of sapphire from syenite pegmatites is small, although gems were extracted from these rocks in Russia, Canada, India and Norway (Giuliani *et al.* 2014). This issue reveals the importance of the rare pegmatites presented here in our research.

4.b.3. The importance of zircon geochemistry

The chemical affinities of zircon grains of the SBPs show some similarities to and some differences with zircon grains of syenites, granitoids and pegmatites elsewhere in the world (Fig. 13). As is visible in Figure 13, some samples plot outside fields indicated

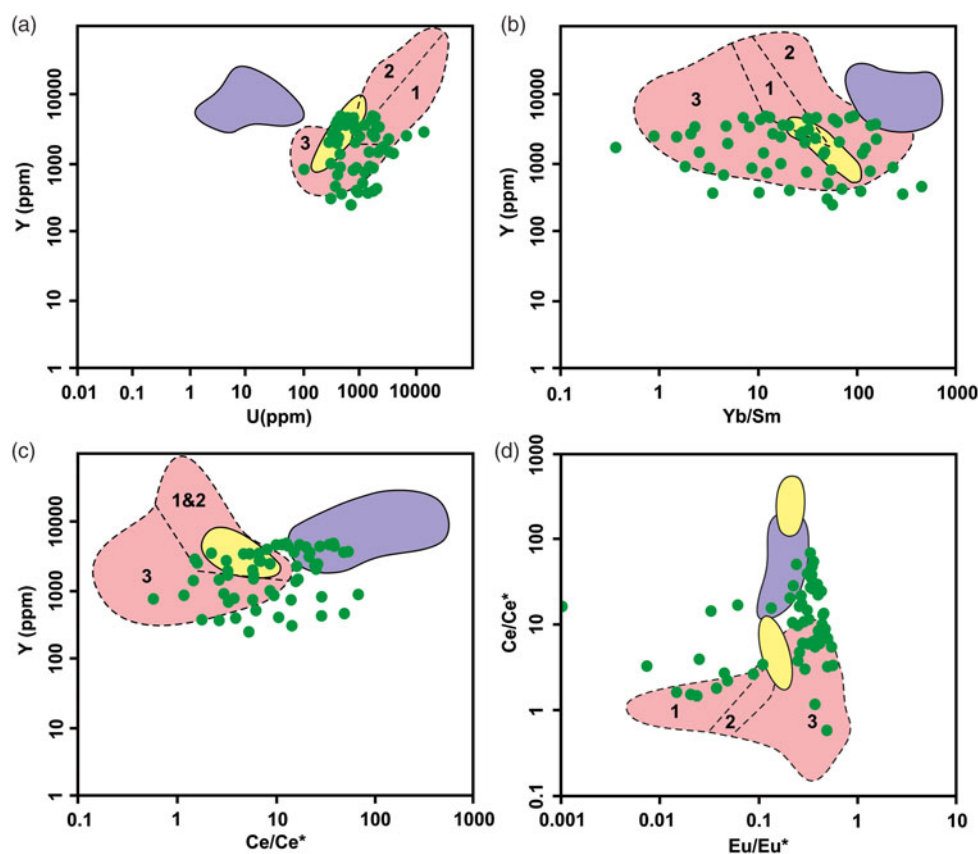


Fig. 15. (Colour online) Plot of chemical compositions of the studied zircon grains for comparison with other zircons of granitoids and pegmatites of other localities (drawn fields after Belousova *et al.* 2002): (a) Y vs U; (b) Y vs Yb/Sm; (c) Y vs Ce/Ce*; (d) Ce/Ce* vs Eu/Eu*. Yellow fields: syenite pegmatites; purple field: nepheline syenite and syenite pegmatites; pink fields: granitoids – (1) aplites, leucogranites; (2) granites; (3) granodiorites and tonalites.

for zircons studied by Belousova *et al.* (2002). The differences are most probably due to the unique composition of these rocks, especially those that have low silica and high alumina contents in contrast to their other known equivalents. Also, early crystallization of zircon grains may affect its geochemical affinity, such as Zr/Hf ratios as well as contents of various trace elements in the composition of zircon (see Section 3.g). On the whole, the studied zircon grains show characteristics of magmatic zircons in contrast to hydrothermal zircons, although some grains plot outside the field of previously studied magmatic zircons. Pronounced positive Ce anomalies in zircons are in accordance with this result. In diagrams for distinguishing the environment of generation for zircons, nearly all studied zircons plot in the field of continental zircons (Fig. 12; Grimes *et al.* 2007).

4.c. Geodynamics remarks

Pegmatites intrude plutonic and metamorphic host rocks in many parts of the SSZ, Iran. Their outcrops are hosted by several plutonic complexes such as Boroujerd, Alvand (Hamedan) and Qorveh (Fig. 1). Masoudi (unpub. PhD, Univ. Leeds, 1997), Masoudi *et al.* (2002) and Ahmadi-Khalaji *et al.* (2007) have studied the petrology and geochronology of pegmatites and associated plutonic and metamorphic rocks from the Boroujerd area in the SSZ. These authors attributed pegmatite development to Mesozoic magmatism. Recently, Salami (unpub. PhD, Bu-Ali Sina Univ., Hamedan, 2017) and Sepahi *et al.* (2018) carried out petrological and geochronological studies on pegmatites and aplites of three main areas in the SSZ (i.e. the Boroujerd, Hamedan and Qorveh areas; Fig. 1). These researches revealed the importance of Mesozoic plutonism and pegmatite genesis in the northwest of the SSZ. The studied pegmatites mainly belong to the LCT class of pegmatites, and

mineralogically they are MSREL pegmatites. These types of pegmatites that contain boron-rich minerals, such as tourmaline in most places, are related to S-type granitoids having an anatectic origin. Sepahi (unpub. PhD, Tarbiat Moallem Univ. Tehran, 1999; 2008) found a genetic relationship between pegmatites–aplites and granitoids (granite–granodiorite) of the Alvand plutonic complex in the Hamedan region.

Northwest of SSZ a spectrum of granitoid types is present including I-, S-, M- and A-type. Plutonic bodies, of which substantial parts are granitoids, occur in many localities, such as Hasanrobat (Muteh) (Alirezai & Hassanzadeh, 2012), Aligoudarz (Esna-Ashari *et al.* 2012), Azna (Moazzen *et al.* 2004), Boroujerd (Ahmadi-Khalaji *et al.* 2007), Malayer (Samen) (Ahadnejad *et al.* 2011), Alvand (Hamedan) (Sepahi 2008; Shahbazi *et al.* 2010), Almoghollah (Shahbazi *et al.* 2015) and Qorveh (Yajam *et al.* 2015). Granitic pegmatites and aplites are not volumetrically large in some of these bodies, but they can be important in the interpretation of the tectono-magmatic history of the region as their host granitoids.

Most granitoids of the Alvand plutonic complex are I-type (including M-type) and S-type, but in adjacent regions, such as Qorveh, A-type granitoids also occur (Sepahi, unpub. PhD, Tarbiat Moallem Univ. Tehran, 1999; Sarjoughian *et al.* 2016). Granitic pegmatites of the region also have various typologies as their associated granitoids. Both the LCT and niobium–yttrium–fluorine (NYF) family of pegmatites occur northwest of the SSZ, indicating complex geodynamic processes in this zone (Salami, unpub. PhD, Bu-Ali Sina Univ., Hamedan, 2017). Also, the aluminium saturation index (ASI) of pegmatites varies from peraluminous to metaluminous and peralkaline. Therefore, this zone must have been affected by various stages of compression and extension during Mesozoic time to produce different types of magmas, from subalkaline to alkaline and peralkaline. These magmas

Table 4. Zircon and monazite saturation temperatures for various granitoids, SBPs and other pegmatites

Sample No.	Rock type	Number	T_{Zircon} (°C)	Min-Max-(Ave) T (°C)	T_{Monazite} (°C)	Min-Max-(Ave) T (°C)
SMV-206	Granitoid		828		827	
SMV-197	Granitoid		815		807	
SMV-194	Granitoid		735		734	
SMV-190	Granitoid		644		702	
SMV-182	Granitoid		802		801	
ME-418	Granitoid		822		807	
ME-415	Granitoid		841		845	
ME-108	Granitoid		834		869	
ME-414	Granitoid		870		816	
ME-429	Granitoid		831		839	
ME-417	Granitoid		818		818	
RMK-A-1	Granitoid		789		794	
RMK-B-5	Granitoid		801		813	
RMK-B	Granitoid		821		841	
RMK-C-7	Granitoid		802		816	
RMK-D-51	Granitoid		817		831	
M-1	Granitoid		795		802	
M-4	Granitoid		802		807	
M-8	Granitoid		802		814	
Total	Granitoids	19	–	644-870-(804)	–	702-869-(810)
SMV-1	Sapphire-bearing pegmatite		635		770	
SMV-131	Sapphire-bearing pegmatite		615		739	
SMV-131b	Sapphire-bearing pegmatite		614		735	
Total	Sapphire-bearing pegmatites	3	–	614-635-(621)	–	735-770-(748)
SMV-204	Other pegmatite		648		689	
SMV-195	Other pegmatite		669		650	
SMV-175	Other pegmatite		614		579	
ME-6	Other pegmatite		729		679	
ME-413	Other pegmatite		635		598	
RMK-D-5	Other pegmatite		832		843	
Total	Other pegmatites	6	–	614-832-(688)	–	579-843-(673)

have resulted in diverse plutonic rocks, especially granitoids and granitic pegmatites, after solidification at different levels in the crust. The LCT pegmatites that occur in orogenic belts have commonly originated from reworking or exhumation of continental crust in high-grade metamorphic terrains.

Among various tectono-magmatic events in the SSZ, plutonism in the Jurassic (giving rise to the formation of granitoids and granitic pegmatites) is volumetrically significant in the northwestern parts of this zone (especially in the Hamedan region; e.g. Shahbazi *et al.* 2010; Sepahi *et al.* 2018). As noted in some publications, both compressional and extensional tectonic regimes are considered to have caused such magmatism in the region (e.g. Shahbazi *et al.* 2015; Sarjoughian *et al.* 2016). The studied pegmatites and their host granitoids show signatures of rocks formed in orogenic

systems, so we emphasize that Jurassic magmatism of the region has been induced during orogenesis.

5. Conclusions

Notable pegmatitic and aplitic rocks in the region have field, petrographic and geochemical features that indicate the existence of a genetic link between them and granitoids of the region. Most granitoids and pegmatites are mildly peraluminous, but a rare type of silica-undersaturated syenitoid pegmatite is unexpectedly extremely peraluminous ($A/CNK > 2$) and does not show any genetic link with other pegmatites and granitoids. Corundum in the syenitoid pegmatites has an igneous origin, because there are no signs of desilication based on field and petrographic studies. The U–Pb geochronology

indicates a Middle Jurassic age (~165 Ma) for SBPs; an age similar to granitoids and other pegmatites. These rocks and associated granitoids have most probably been generated in an orogenic system.

Zircon geochemistry shows that zircon grains are rich in notable incompatible elements, such as Hf (up to 17 200 ppm), U (up to 13 580 ppm), Th (up to 5148 ppm), Y (up to 4764 ppm) and Σ REE (up to 2534 ppm), with a distinct positive correlation between Y and HREE contents. The Zr/Hf ratio of zircons is accordant with early crystallization from magma. Also, there is a negative correlation between Hf and Y and HREE values, but Nb-Ta, U-Th and Hf-U element pairs show a positive correlation. Zircons show a distinct Ce positive anomaly possibly due to a relatively oxidized condition of the magma from which zircon crystallized. Ti-in-zircon thermometry yields a temperature range of ~683 to ~828 °C (avg 755 ± 73 °C) for crystallization of zircon grains. The T_{zircon} for the sapphire-bearing syenitoid pegmatites is in the range 614–635 °C with an average of 622 °C, similar to the other pegmatites' T_{zircon} ranging from 614 to 832 °C (avg. 688 °C). These lower fractionation temperatures are consistent with crystallization temperatures of other magmatic zircons in pegmatites of previously published studies. Zircons have properties of continental zircons.

Acknowledgements. We thank Lorence G. Collins for editing an earlier version of the manuscript. We acknowledge Acme Analytical Laboratories, Vancouver, Canada, for ICP-MS and ICP-ES analyses on whole rock samples. Also, we appreciate the micro-XRF and LA-ICP-MS lab of the University of New Brunswick for carrying out precise analyses on zircon grains. David Lentz and Chris McFarlane are supported by NSERC Discovery grants.

Supplementary material. To view supplementary material for this article, please visit <https://doi.org/10.1017/S0016756820000023>

References

- Ahadnejad, V, Valizadeh, MV, Deevsalar, R and Rezaei-Kahkhaei, M (2011) Age and geotectonic position of the Malayer granitoids: implication for plutonism in the Sanandaj-Sirjan zone, W Iran. *Neues Jahrbuch für Geologie und Paläontologie – Abhandlungen* **261**, 61–75.
- Ahmadi-Khalaji, A, Esmaili, D, Valizadeh, MV and Rahimpour-Bonab, H (2007) Petrology and geochemistry of the granitoid complex of Boroujerd, Sanandaj-Sirjan zone, Western Iran. *Journal of Asian Earth Sciences* **29**, 859–77.
- Alavi, M (1994) Tectonics of Zagros orogenic belt of Iran: new data and interpretation. *Tectonophysics* **229**, 211–38.
- Alavi, M (2004) Regional stratigraphy of the Zagros fold-thrust belt of Iran and its proforeland evolution. *American Journal of Science* **304**, 1–20.
- Alfonso, P, Melgarejo, JC, Yusta, I and Velasco, F (2003) Geochemistry of feldspars and muscovite in granitic pegmatite from the Cap de Creus field, Catalonia, Spain. *Canadian Mineralogist* **41**, 103–16.
- Aliani, F, Maanijou, M, Sabouri, Z and Sepahi, AA (2012) Petrology, geochemistry and geotectonic environment of the Alvand intrusive complex, Hamedan, Iran. *Chemie der Erde* **72**, 363–83.
- Alirezai, S and Hassanzadeh, J (2012) Geochemistry and zircon geochronology of the Permian A-type Hasanrobat granite, Sanandaj-Sirjan belt: a new record of the Gondwana break-up in Iran. *Lithos* **151**, 122–34.
- Babazadeh, S, Ghorbani, MH, Cottle, JM and Bröcker, M (2019) Multistage tectono-magmatic evolution of the central Urumieh–Dokhtar magmatic arc, south Ardestan, Iran: insights from zircon geochronology and geochemistry. *Geological Journal* **54**, 1–25.
- Baharifar, A, Moinevaziri, H, Bellon, H and Piqué, A (2004) The crystalline complexes of Hamadan (Sanandaj–Sirjan zone, western Iran): metasedimentary Mesozoic sequences affected by Late Cretaceous tectono-metamorphic and plutonic events. *Comptes Rendus Geoscience* **336**, 1443–52.
- Ballard, JR, Palin, MJ and Campbell, IH (2002) Relative oxidation states of magmas inferred from Ce(IV)/Ce(III) in zircon: application to porphyry copper deposits of northern Chile. *Contributions to Mineralogy and Petrology* **144**, 347–64.
- Belousova, EA, Griffin, WL, O'Reilly, SY and Fisher, NI (2002) Igneous zircon: trace element composition as an indicator of source rock type. *Contributions to Mineralogy and Petrology* **143**, 602–22.
- Boynnton, WV (1984) Cosmochemistry of the rare earth elements meteorite studies. In *Rare Earth Element Geochemistry* (ed. P Henderson), pp. 63–114. Amsterdam: Elsevier.
- Breiter, K, Lamarão, CN, Borges, RMK and Dall'Agnol, R (2016) Chemical characteristics of zircon from A-type granites and comparison to zircon of S-type granites. *Lithos* **192–195**, 208–25.
- Cerný, P and Ercit, TS (2005) The classification of granitic pegmatites revisited. *Canadian Mineralogist* **43**, 2005–26.
- Cerný, P, London, D and Novak, M (2012) Granitic pegmatites as reflections of their source. *Elements* **8**, 289–94.
- Cerný, P, Meintzer, RE and Anderson, AJ (1985) Extreme fractionation in rare-element granitic pegmatites: selected examples of data and mechanisms. *Canadian Mineralogist* **23**, 381–421.
- Chappell, BW and White, AJR (1992) I and S-type granites in the Lachlan Fold belt. *Transactions of the Royal Society of Edinburgh: Earth Sciences* **83**, 1–26.
- Chiu, HY, Chung, SL, Zarrinkoub, MH, Mohammadi, SS, Khatib, MM and Iizuka, Y (2013) Zircon U–Pb age constraints from Iran on the magmatic evolution related to Neotethyan subduction and Zagros orogeny. *Lithos* **162–163**, 70–87.
- Christiansen, EH and Keith, JD (1996) Trace element systematics in granitic magmas: a metallogenic perspective. *Geological Association of Canada Short Course* **12**, 115–51.
- Cox, KG, Bell, JD and Pankhurst, RJ (1979) *The Interpretation of Igneous Rocks*. London: Allen & Unwin, 450 pp.
- Dill, HG (2015) Pegmatites and aplites: their genetic and applied ore geology. *Ore Geology Reviews* **69**, 417–561.
- Dill, HG (2016) The CMS classification scheme (Chemical composition–Mineral assemblage–Structural geology) – linking geology to mineralogy of pegmatitic and aplitic rocks. *Neues Jahrbuch für Mineralogie – Abhandlungen / Journal of Mineralogy and Geochemistry* **193**, 231–63.
- Eсна-Ashari, A, Tiepolo, M, Valizadeh, MV, Hassanzadeh, J and Sepahi, AA (2012) Geochemistry and zircon U–Pb geochronology of Aligoodarz granitoid complex, Sanandaj-Sirjan zone, Iran. *Journal of Asian Earth Sciences* **43**, 11–22.
- Ferry, JM and Watson, EB (2007) New thermodynamic models and revised calibrations for the Ti-in-zircon and Zr-in-rutile thermometers. *Contributions to Mineralogy and Petrology* **154**, 429–37.
- Flude, S, Haschke, M and Storey, M (2017) Application of benchtop micro-XRF to geological materials. *Mineralogical Magazine* **81**, 923–48.
- Fu, B, Page, FZ, Cavosie, AJ, Fournelle, J, Kita, NT, Lackey, JS, Wilde, SA and Valley, JW (2008) Ti-in-zircon thermometry: applications and limitations. *Contributions to Mineralogy and Petrology* **156**, 197–215.
- Gao, P, Zheng, YF and Zhao, ZF (2016) Distinction between S-type and peraluminous I-type granites: zircon versus whole-rock geochemistry. *Lithos* **258–259**, 77–91.
- Ghasemi, A and Talbot, CJ (2006) A new tectonic scenario for the Sanandaj-Sirjan zone (Iran). *Journal of Asian Earth Sciences* **26**, 683–93.
- Giuliani, G, Fallick, A, Ohnenstetter, D and Pegere, G (2009) Oxygen isotopes composition of sapphires from the French Massif Central: implications for origin of gem corundum in basaltic fields. *Mineralium Deposita* **44**, 221–31.
- Giuliani, G, Fallick, A, Rakotondrazafy, M, Ohnenstetter, D, Andriamamonjy, A, Ralantoarison, T, Rakotosamizany, S, Razanatseno, M, Offant, Y, Garnier, V, Dunaigre, C, Schwarz, D, Mercier, A, Ratrimo, V and Ralison, B (2007) Oxygen isotope systematic of gem corundum deposits in Madagascar: relevance for their geological origin. *Mineralium Deposita* **42**, 251–70.
- Giuliani, G, Fallick, AE, Garnier, V, France-Lanord, C, Ohnenstetter, D and Schwarz, D (2005) Oxygen isotope composition as a tracer for the origins of rubies and sapphires. *Geology* **33**, 249–52.
- Giuliani, G, Ohnenstetter, D, Fallick, AE, Groat, L and Fagan, AJ (2014) The geology and genesis of gem corundum deposits. *Mineralogical Association of Canada Short Course* **44**, 29–112.

- Graham, I, Sutherland, L, Zaw, K, Nechaev, V and Khanchuk, A (2008) Advances in our understanding of the gem corundum deposits of the West Pacific continental margins intraplate basaltic fields. *Ore Geology Reviews* **34**, 200–15.
- Grimes, CB, John, BE, Kelemen, PB, Mazdab, FK, Wooden, JL, Cheadle, MJ, Hanghøj, K and Schwartz, JJ (2007) Trace element chemistry of zircons from oceanic crust: a method for distinguishing detrital zircon provenance. *Geology* **35**, 643–6.
- Hanson, SL (2016) A tectonic evaluation of pegmatite parent granites. *Canadian Mineralogist* **54**, 917–33.
- Harley, SL and Kelly, NM (2007) Zircon tiny but timely. *Elements* **3**, 13–18.
- Harrison, TM, Aikman, A, Holden, P, Walker, AM, McFarlane, C, Rubatto, D and Watson, EB (2005) Testing the Ti-in-zircon thermometer. *Eos, Transactions, American Geophysical Union, Abstract* **86**, V41F–1540.
- Hassanzadeh, J and Wernicke, BP (2016) The Neotethyan Sanandaj-Sirjan zone of Iran as an archetype for passive margin-arc transitions. *Tectonics* **35**, 586–621.
- Hofmann, AE, Baker, MB and Eiler, JM (2014) Sub-micron-scale trace-element distributions in natural zircons of known provenance: implications for Ti-in-zircon thermometry. *Contributions to Mineralogy and Petrology* **168**, 1057. doi: [10.1007/s00410-014-1057-8](https://doi.org/10.1007/s00410-014-1057-8).
- Hoskin, PWO and Schaltegger, URS (2003) The composition of zircon and igneous and metamorphic petrogenesis. *Reviews in Mineralogy and Geochemistry* **53**, 27–62.
- Kirkland, CL, Smithies, RH, Taylor, RJM, Evans, N and McDonald, B (2015) Zircon Th/U ratios in magmatic environs. *Lithos* **212–215**, 397–414
- London, D (2005) Granitic pegmatites: an assessment of current concepts and directions for the future *Lithos* **80**, 281–303.
- London, D (2008) *Pegmatites*. Canadian Mineralogist, Special Publication 10. Quebec: Mineralogical Association of Canada, 347 pp.
- London, D (2014a) A petrologic assessment of internal zonation in granitic pegmatite. *Lithos* **184–187**, 74–104.
- London, D (2014b) Subsolidus isothermal fractional crystallization. *American Mineralogist* **99**, 543–6.
- London, D (2018) Ore-forming processes within granitic pegmatites. *Ore Geology Reviews* **101**, 349–83.
- London, D and Morgan, G, VI (2012) The pegmatite puzzle. *Elements* **8**, 263–8.
- Ludwig, KR (2003) *User's Manual for Isoplot/Ex, Version 3.0. A Geochronological Toolkit for Microsoft Excel*. Berkeley, CA: Berkeley Geochronology Center, Special Publication, v.4.
- Mahmoudi, S, Corfu, F, Masoudi, F, Mehrabi, B and Mohajjel, M (2011) U–Pb dating and emplacement history of granitoid plutons in the northern Sanandaj–Sirjan zone, Iran. *Journal of Asian Earth Sciences* **41**, 238–49.
- Maniar, PD and Piccoli, PM (1989) Tectonic discrimination of granitoids. *Geological Society of America Bulletin* **10**, 635–43.
- Masoudi, F, Yardley, BWD and Cliff, RA (2002) Rb–Sr geochronology of pegmatites, plutonic rocks and a hornfels in the region south-west of Arak, Iran. *Journal of Sciences of the Islamic Republic of Iran* **13**, 249–54.
- McFarlane, C and Luo, Y (2012) U–Pb geochronology using 193 nm Excimer LA–ICP–MS optimized for in situ accessory mineral dating in thin sections. *Geoscience Canada* **39**, 158–72.
- Mehdipour-Ghazi, J and Moazzen, M (2015) Geodynamic evolution of the Sanandaj-Sirjan Zone, Zagros Orogen, Iran. *Turkish Journal of Earth Sciences* **24**, 513–28.
- Middlemost, EAK (1994) Naming material in the magma/igneous rock system. *Earth-Science Reviews* **37**, 215–24.
- Moazzen, M, Moayyed, M, Modjarrad, M and Darvishi, E (2004) Azna granitoid as an example of syn-collision S-type granitisation in Sanandaj-Sirjan metamorphic belt, Iran. *Neues Jahrbuch für Mineralogie – Monatshefte* **2004**, 489–507.
- Mohajjel, M and Fergusson, C L (2014) Jurassic to Cenozoic tectonics of the Zagros Orogen in northwestern Iran. *International Geology Review* **56**, 263–87.
- Montel, J M (1993) A model for monazite/melt equilibrium and application to the generation of granitic magmas. *Chemical Geology* **110**, 127–46.
- Nabelek, P I, Whittington, AG and Sirbescu, MC (2010) The role of H₂O in rapid emplacement and crystallization of granite pegmatites: resolving the paradox of large crystals in highly undercooled melts. *Contributions to Mineralogy and Petrology* **160**, 313–25.
- Nardi, LVS, Formoso, MLL, Müller, IF, Fontana, E, Jarvis, K and Lamarão, C (2013) Zircon/rock partition coefficients of REEs, Y, Th, U, Nb, and Ta in granitic rocks: uses for provenance and mineral exploration purposes. *Chemical Geology* **335**, 1–7.
- Nouri, F, Stern, RJ and Azizi, H (in press) The Jurassic tourmaline-garnet-beryl semi-gemstone province in the Sanandaj-Sirjan zone, Western Iran. *International Geology Review* 1–25.
- Pearce, JA, Harris, NB and Tindle, AG (1984) Trace element discrimination diagrams for the tectonic interpretation of granitic rocks. *Journal of Petrology* **25**, 956–83.
- Sarjoughian, F, Kananian, A, Haschke, M and Ahmadian, J (2016) Transition from I-type to A-type magmatism in the Sanandaj-Sirjan zone, NW Iran: an extensional intra-continental arc. *Geological Journal* **51**, 387–404.
- Sepahi, AA (2008) Typology and petrogenesis of granitic rocks in the Sanandaj-Sirjan metamorphic belt, Iran: with emphasis on the Alvand plutonic complex. *Neues Jahrbuch für Geologie und Paläontologie* **247**, 295–312.
- Sepahi, AA and Athari, SF (2006) Petrology of major granitic plutons of the northwestern part of the Sanandaj-Sirjan metamorphic belt, Zagros orogen, Iran: with emphasis on A-type granitoids from the SE Saqqez area. *Neues Jahrbuch für Mineralogie – Abhandlungen: Journal of Mineralogy and Geochemistry* **183**, 93–106.
- Sepahi, AA, Jafari, SR and Mani-Kashani, S (2009) Low pressure migmatites from the Sanandaj-Sirjan Metamorphic Belt in the Hamedan region (Iran). *Geologica Carpathica* **60**, 107–19.
- Sepahi, AA, Jafari, SR, Osanai, Y, Shahbazi, H and Moazzen, M (2019) Age, petrologic significance and provenance analysis of the Hamedan low-pressure migmatites, Sanandaj-Sirjan zone, west Iran. *International Geology Review* **61**, 1446–61.
- Sepahi, AA, Salami, S, Lentz, D, McFarlane, C and Maanjou, M (2018) Petrography, geochemistry, and U–Pb geochronology of pegmatites and aplites associated with Alvand intrusive complex in Hamedan region, Sanandaj-Sirjan zone, Zagros orogen (Iran). *International Journal of Earth Sciences* **107**, 1059–96.
- Sepahi, AA, Whitney, DL and Baharifar, AA (2004) Petrogenesis of andalusite-kyanite-sillimanite veins and host rocks, Sanandaj-Sirjan metamorphic belt, Hamadan, Iran. *Journal of Metamorphic Geology* **22**, 119–34.
- Shahbazi, H, Siebel, W, Ghorbani, M, Pourmoafee, M, Sepahi, AA, Vousoughi-Abedini, M and Shang, CK (2015) The Almogholagh pluton, Sanandaj-Sirjan zone, Iran: geochemistry, U–(Th)–Pb titanite geochronology and implications for its tectonic evolution. *Neues Jahrbuch für Mineralogie – Abhandlungen / Journal of Mineralogy and Geochemistry* **192**, 85–99.
- Shahbazi, H, Siebel, W, Pourmoafee, M, Ghorbani, M, Sepahi, AA, Shang, CK and Vousoughi-Abedini, M (2010) Geochemistry and U–Pb zircon geochronology of the Alvand plutonic complex in Sanandaj–Sirjan zone (Iran): new evidence for Jurassic magmatism. *Journal of Asian Earth Sciences* **39**, 668–83.
- Shand, SJ (1943) *Eruptive Rocks, Their Genesis, Composition, Classification and Their Relation to Ore Deposits*. New York: Wiley, 444 pp.
- Sheikhi-Gheshlaghi, R and Ahmadi, M H (2015) Pegmatites characteristics of south Hamedan: corundums gemological approach. *Geochemistry* **4**, 269–82 (in Persian).
- Shen, P, Hattori, K, Pan, H, Jackson, S and Seitmuratova, E (2015) Oxidation condition and metal fertility of granitic magmas: zircon trace-element data from porphyry Cu deposits in the Central Asian Orogenic Belt. *Economic Geology* **110**, 1861–78.
- Simmons, WB and Webber, KL (2008) Pegmatite genesis: state of the art. *European Journal of Mineralogy* **20**, 421–38.
- Simonet, C, Fritsch, E and Lasnier, B (2008) A classification of gem corundum deposits aimed towards gem exploration. *Ore Geology Reviews* **34**, 27–133.
- Simonet, C, Paquette, J L, Pin, C, Lasnier, B and Fritsch, E (2004) The Dusi (Garba Tula) sapphire deposit, Central Kenya: a unique Pan-African corundum-bearing monzonite. *Journal of African Earth Sciences* **38**, 401–10.
- Smythe, DJ and Brenan, JM (2016) Magmatic oxygen fugacity estimated using zircon-melt partitioning of cerium. *Earth Planetary Science Letters* **453**, 260–6.
- Stocklin, J and Setudenia, A (1972) *Lexique stratigraphique international, vol. III*. Paris: Centre National de la Recherche Scientifique, 75 pp.

- Sutherland FL, Duroc-Danner, JM and Meffre, S** (2008) Age and origin of gem corundum and zircon megacrysts from the Mercaderes-Rio Mayo area, South-West Colombia, South America. *Ore Geology Reviews* **34**, 155–68.
- Takin, M** (1972) Iranian geology and continental drift in the Middle East. *Nature* **235**, 147–50.
- Thomas, R and Davidson, P** (2015) Comments on “A petrologic assessment of internal zonation in granitic pegmatites” by David London 2014. *Lithos* **212–221**, 462–8.
- Thomas, R, Davidson, P and Beurlen, H** (2012) The competing models for the origin and internal evolution of granitic pegmatites in the light of melt and fluid inclusion research. *Mineralogy and Petrology* **106**, 55–73.
- Trail, D, Watson, EB and Tailby, ND** (2012) Ce and Eu anomalies in zircon as proxies for the oxidation state of magmas. *Geochimica et Cosmochimica Acta* **97**, 70–87.
- Uher, P, Giuliani, G, Szakall, S, Fallick, A, Strunga, V, Vaculovic, T, Ozdin, D and Greganova, M** (2012) Sapphires related to alkali basalts from the Cerova Highlands, Western Carpathians (Southern Slovakia): composition and origin. *Geologica Carpathica* **63**, 71–82.
- Valizadeh, MV and Cantagrel, JM** (1975) Premières données radiométriques (K–Ar et Rb–Sr) sur les micas du complexes magmatique du Mont Alvand, Pres Hamadan (Iran occidental). *Comptes Rendus de l'Academie des Sciences, Paris* **281**, 1083–6.
- Wang, X, Griffin, WL and Chen, J** (2010) Hf contents and Zr/Hf ratios in granitic zircons. *Geochemical Journal* **44**, 65–72.
- Watson, EB and Harrison TM** (1983) Zircon saturation revisited: temperature and composition effects in a variety of crustal magma types. *Earth and Planetary Science Letters* **64**, 295–304.
- Watson, EB and Harrison, TM** (2005) Zircon thermometer reveals minimum melting conditions on earliest Earth. *Science* **308**, 841–44.
- Watson, EB, Wark, DA and Thomas, JB** (2006) Crystallization thermometers for zircon and rutile. *Contributions to Mineralogy and Petrology* **151**, 413–33.
- Whitney, DL and Evans, BW** (2010) Abbreviations for names of rock-forming minerals. *American Mineralogist* **95**, 185–7.
- Yajam, S, Montero, P, Scarrow, JH, Ghalamghash, J, Razavi, SMH and Bea, F** (2015) The spatial and compositional evolution of the Late Jurassic Ghorveh–Dehgolan plutons of the Zagros orogen, Iran: SHRIMP zircon U–Pb and Sr and Nd isotope evidence. *Geologica Acta* **13**, 25–43.
- Yang, TN, Chen, JL, Liang, MJ, Xin, D, Aghazadeh, M, Hou, Z and Zhang, HR** (2018) Two plutonic complexes of the Sanandaj–Sirjan magmatic–metamorphic belt record Jurassic to Early Cretaceous subduction of an old Neotethys beneath the Iran microplate. *Gondwana Research* **62**, 246–68.
- Yang, XM, Lentz, DR, Chi, G and Thorne, KG** (2008) Geochemical characteristics of gold-related granitoids in southwestern New Brunswick, Canada. *Lithos* **104**, 355–77.
- Zhang, H, Chen, J, Yang, T, Hou, Z and Aghazadeh, M** (2018a) Jurassic granitoids in the northwestern Sanandaj–Sirjan zone: evolving magmatism in response to the development of a Neo-Tethyan slab window. *Gondwana Research* **62**, 269–86.
- Zhang, Z, Xiao, W, Ji, WQ, Majidifard, MR, Rezaeian, M, Talebain, M, Xiang, D, Chen, L, Wan, B, Ao, S and Esmaceli, R** (2018b) Geochemistry, zircon U–Pb and Hf isotope for granitoids, NW Sanandaj–Sirjan zone, Iran: implications for Mesozoic–Cenozoic episodic magmatism during Neo-Tethyan lithospheric subduction. *Gondwana Research* **62**, 227–45.